*Original Research*

The Effects of Dexamethasone on Human Lens Epithelial Cells and the Analysis of Related Pathways with Transcriptome Sequencing

Xinjie Shu[1] , Jiamin Gao[1,2], Han Xu[1,2], Qiyou Li[3], Yu Gong[1],*,† , Jiawen Li[1,2],*,†

[1]Department of Ophthalmology, University-Town Hospital of Chongqing Medical University, 401331 Chongqing, China
[2]Department of Ophthalmology and Optometry, Chongqing Medical University, 401331 Chongqing, China
[3]Department of Ophthalmology, Southwest Hospital/Southwest Eye Hospital, Third Military Medical University (Army Medical University), 400038 Chongqing, China
*Correspondence: gongyu@hospital.cqmu.edu.cn (Yu Gong); 800396@hospital.cqmu.edu.cn (Jiawen Li)
†These authors contributed equally.

Abstract

Background: The goal of this study was to investigate the effects of dexamethasone on human lens epithelial cells (HLECs) and the potential mechanisms. **Methods**: HLECs (HLE-B3) were cultured *in vitro* to assess the effects of dexamethasone on cell size at different concentrations. Immunofluorescence staining was used to detect specific protein expression in HLE-B3 cells. The cell size was observed using phase-contrast microscopy, and the length and area were quantitatively measured with ImageJ software for statistical analysis. Flow cytometry was used to verify these outcomes. The means of three groups were statistically analyzed using one-way analysis of variance, whereas the means of two groups were statistically analyzed with the parametric Student's *t*-test. Additionally, high-throughput transcriptome sequencing was performed to compare messenger RNA (mRNA) expression levels between different concentrations of dexamethasone treatment groups and the control group, to identify potential signaling pathways. Subsequently, we performed quantitative Polymerase Chain Reaction (qPCR), immunofluorescence staining, and molecular docking experiments on the key differentially expressed genes. **Results**: Dexamethasone affected the size of HLE-B3 cells. Both 0.25 and 0.5 µmol/L dexamethasone increased cell length and area, exhibiting no significant difference between the two treatment groups. Flow cytometry showed that dexamethasone increased cell size and granularity, with 0.25 µmol/L dexamethasone leading to larger cell areas and higher intracellular granularity. High-throughput transcriptome sequencing revealed significant upregulation of lysophosphatidic acid receptor 1 (LPAR1) and the pathways related to the glucocorticoid (GC) receptor. **Conclusions**: Certain concentrations of dexamethasone impact the morphology and biological functions of HLECs. As a subtype of G protein-coupled receptors, LPAR1 on the cell membrane may interact with dexamethasone, affecting cell size and inhibiting autophagy via the phosphoinositide 3-kinase (PI3K)/protein kinase B (AKT)/mammalian target of rapamycin (mTOR) pathway. These discoveries offer crucial biological insights into how dexamethasone influences the morphology and function of HLECs and the pathogenesis of GC-induced cataracts, offering potential molecular targets for future therapeutic strategies.

Keywords: glucocorticoid-induced cataracts; dexamethasone; lens epithelial cells; transcriptome sequencing; lysophosphatidic acid receptor 1

1. Introduction

Cataracts are the primary cause of blindness globally, affecting 17.2% of people worldwide [1,2]. Glucocorticoids (GCs) are a kind of drugs widely used to treat inflammation, autoimmune diseases, and certain cancers. However, long-term or high-dose GC therapy is associated with a variety of adverse effects, and posterior subcapsular opacities of the lens is one of its common side effects in ophthalmology, known as induced GC-induced cataracts (GIC). Its prevalence is about 14% to 16% of all cataracts [3]. Black *et al*. [4] first suggested in 1960 that GC is closely related to cataracts development. Since then, a large amount of epidemiological and clinical data has confirmed that long-term large amounts of oral, inhalation, and ocular surface drops of GCs and intraocular injection of GC extended-release agents can cause cataracts [5–8]. Surgery can improve vi-

sion in patients with cataracts, but carries financial costs [9] and some postoperative complications such as dry eye or macular cystoid edema, and increases the risk of posterior capsular opacification and endophthalmitis [10,11]. Unlike diabetes mellitus and age-related cataract (ARC), GIC severely restrict the fine vision requirements of young and middle-aged patients, and even post-cataract surgery, the visual quality may not be comparable to that of normal eyes [12]. Consequently, research into the precise molecular pathways underlying GIC is imperative.

Lens epithelial cells (LECs) play a significant role in regulating the transparency of lens, and abnormalities in the morphology and function of these cells can lead to cataracts. Dexamethasone, a classic GC used clinically, can cause morphological changes in LECs including cellular disorganization and vacuolization of intercellular junctions by decreasing waveform protein expression [13]; cellular edema

Publisher's Note: IMR Press stays neutral with regard to jurisdictional claims in published maps and institutional affiliations.

by inhibiting the Na^+/K^+-ATPase enzyme [14]; and cellular loss of polarity, reduction of adhesion function, hyperproliferation, and migration by lack of calcineurin [15]. These effects, in turn, cause functional abnormalities in LECs; however, the precise cellular and molecular mechanisms in humans are not fully understood. Therefore, to determine the effects of dexamethasone on human lens epithelial cells (HLECs) and the underlying mechanism, we employed high-throughput transcriptome sequencing to search for the potential molecular pathways.

In the messenger RNA (mRNA) expression profiles from transcriptome sequencing, we found that lysophosphatidic acid receptor 1 (LPAR1), as a hub gene in the transcriptomic changes following dexamethasone treatment, was significantly upregulated along with phosphoinositide 3-kinase/protein kinase B (AKT) pathway expression, which is one of the pathways through which dexamethasone affects the function of LECs [16]. LPAR1, a subtype of G protein-coupled receptors (GPCRs), is involved in cellular survival, proliferation, adhesion, migration, and cytoskeletal alterations. As part of the GPCR superfamily, LPAR1 triggers the activation of the phosphoinositide 3-kinase (PI3K)/AKT signaling pathway by interacting with $G\alpha i/o$ proteins. In rodent Schwann cells, one of the most prominent functions of LPAR1-induced $G\alpha i/o$ protein activation is survival signaling through the PI3K/AKT pathway [17]. A recent study has shown that dexamethasone activates adhesion GPCR G3 (also known as GPR97), a prototypical adhesion GPCR [18]. However, it has not been determined whether dexamethasone interacts with LPAR1 and thus affects the cell size and biological functions of HLECs.

Our study investigated the mechanisms and potential signaling pathways that influence the morphology and function of HLECs upon the potential connection of dexamethasone with LPAR1.

2. Materials and Methods

2.1 Experimental Workflow

The experimental workflow for this study is illustrated in Fig. 1.
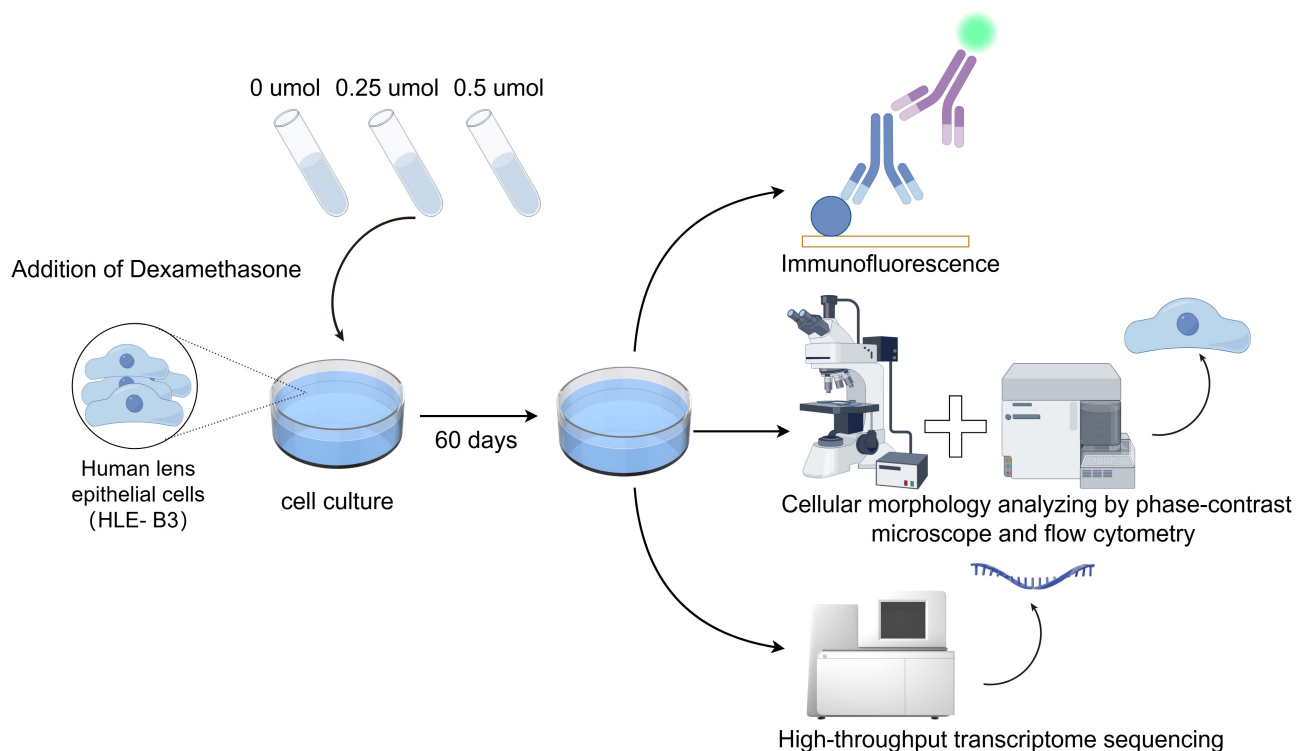
2.2 Cell Culture

The HLE-B3 cell line was purchased from American Type Culture Collection (ATCC; Manassas, VA, USA), an internationally recognized institution that provides ethically reviewed cell lines. The ATCC ensures that all cell lines, including the HLE-B3, are obtained and distributed in compliance with ethical standards. An analysis certificate verifying their provenance and quality is in the **Supplementary Materials**. The HLE-B3 cell line is an immortalized HLEC line frequently used to study the biological properties of HLECs and their responses under various conditions. HLE-B3 cells exhibit stable proliferation and a prolonged lifespan, making them widely used in ophthalmic research, par-

ticularly in studies related to lens-associated diseases such as cataracts [19]. HLE-B3 cells were cultured in a nutrient-rich Dulbecco's Modified Eagle Medium (Gibco, Waltham, MA, USA) supplemented with 10% fetal bovine serum (FBS; Gibco) and the antibiotics penicillin (100 U/mL) and streptomycin (100 µg/mL). These cells were cultured at 37 °C with 5% CO_2. Regular mycoplasma screening was carried out using the MycoAlert Detection Kit (Lonza, Walkersville, MD, USA) to verify the absence of mycoplasma contamination and the test result is negative. Furthermore, the authenticity of the cell line was confirmed through rigorous short tandem repeat (STR) profiling. Authentication and STR profiling were conducted using the Cell Line Authentication Service by ATCC, in accordance with the guidelines of the International Cell Line Authentication Committee (ICLAC) and the ExPASy Cellosaurus database to avoid cross-contamination or misidentification. HLE-B3 cells were divided into three groups: control group with no dexamethasone treatment, 0.25 µmol/L dexamethasone, and 0.5 µmol/L dexamethasone groups. We used HLE-B3 cells treated with 0 µM dexamethasone as the baseline comparison, referred to as the control group, where the cells were treated with the same volume of water used to dissolve the dexamethasone. Each group consist of three samples. All groups were cultured for 60 days, with medium changes and passaging performed weekly.

2.3 Immunofluorescence Staining

After 15 min fixation in 4% paraformaldehyde (Sigma-Aldrich, St. Louis, MO, USA) at room temperature, HLE-B3 cells were permeabilized with 0.1% Triton X-100 (Sigma-Aldrich, St. Louis, MO, USA) for 10 min. Then the cells were blocked in 1% bovine serum albumin (Sigma-Aldrich, St. Louis, MO, USA) for 1 h. Next, HLE-B3 cells were incubated overnight at 4 °C with primary antibodies against α-crystallin, γ-crystallin, and vimentin. After three washes with phosphate-buffered saline (PBS) (Gibco, Thermo Fisher Scientific, Waltham, MA, USA), cells were incubated with fluorophore-tagged secondary antibodies for 1 h in the dark at ambient temperature, followed by additional washing. Then nuclei were stained with 4′,6-diamidino-2-phenylindole (DAPI) for 5 min, followed by coverslip mounting on slides with anti-fade medium. Fluorescence microscopy (Leica, Wetzlar, Germany) was employed to capture the resulting images. Three independent repeat experiments were conducted.

HLE-B3 cells, either untreated or co-cultured with 0.25 µM dexamethasone for 60 days, were fixed for 15 minutes in 4% paraformaldehyde at room temperature. After fixation, cells were permeabilized using 0.1% Triton X-100 for 10 minutes and then blocked with 1% bovine serum albumin (BSA) for 1 hour at room temperature. Cells were incubated overnight at 4 °C with primary antibodies against LPAR1 and phosphorylated S6K1 (p-S6K1). Following three washes with PBS, cells were incubated with appropri-

Fig. 1. Study workflow. This diagram outlines the entire process from cell culture to data analysis. Initially, human lens epithelial cells (HLE-B3) were cultured and treated with different concentrations of dexamethasone (0, 0.25, and 0.5 μM) for 60 days. Subsequent steps included cell size measurement using phase-contrast microscopy, flow cytometry analysis, and high-throughput transcriptome sequencing. By Figdraw (https://www.figdraw.com/#/).

ate fluorophore-conjugated secondary antibodies for 1 hour in the dark at ambient temperature. Nuclei were stained with DAPI for 5 minutes, and coverslips were mounted on slides using anti-fade mounting medium. Fluorescence images were acquired using a fluorescence microscope, and ImageJ software 1.54f (National Institutes of Health, Bethesda, MD, USA) was employed to quantify the fluorescence intensity of LPAR1 and p-S6K1. Three independent repeat experiments were conducted.

2.4 Measurement of Cell Size

Cell size was measured under a phase-contrast microscope (DMI3000B inverted phase contrast microscope; Leica, Wetzlar, Germany) at 2000× magnification. Subsequently, ImageJ software (v.1.54k12) was used to acquire images, which were subjected to analysis for quantification of cellular dimensions. GraphPad Prism (version 10.2.2; GraphPad Software, LLC, La Jolla, CA, USA) was used to statistically analyze the data. For each group, 30 measurements were taken for cell length, and 20 measurements were taken for cell area, cytoplasmic area, nuclear area, and nucleus-cytoplasm ratio.

2.5 Flow Cytometry

Harvested cells were rinsed with PBS, and then resuspended in a modified PBS solution supplemented with 2% FBS. For detailed analysis of cellular dimensions and granularity, we employed the advanced FACSCalibur flow cytometer (BD Biosciences, Franklin Lakes, NJ, USA). FlowJo™ v.10.10 (Tree Star, Ashland, OR, USA) was used for data processing. Three independent repeat experiments were conducted. Flow cytometry analysis focused on assessing changes in cell size and granularity between the control group and the 0.25 μM dexamethasone-treated group, utilizing forward scatter (FSC) and side scatter (SSC) respectively. FSC measurements provide insight into the relative cell size, as FSC correlates with the cell volume or diameter. SSC, on the other hand, measures the granularity or internal complexity of cells, reflecting aspects such as the presence of internal structures like granules. Given the nature of our investigation into the basic cellular responses to dexamethasone, specific markers were not employed in the flow cytometry analysis. The gating strategy and analysis process, detailed in **Supplementary Fig. 1**, was based on guidelines from the FlowJo official gating tutorial. We excluded debris and dead cells by setting appropriate thresholds on FSC and SSC parameters, selecting a population that predominantly represents live HLE-B3.

2.6 High-throughput Transcriptome Sequencing

HLE-B3 cells were cultured *in vitro* and incubated with 0, 0.25, and 0.5 µmol/L dexamethasone for 60 days. Total RNA was extracted from cells with TRIzol® reagent. The integrity and quality of the extracted RNA were assessed utilizing the Agilent 5300 Bioanalyzer (Agilent Technologies, Wilmington, DE, USA). For quantitative analysis, the NanoDrop 2000 spectrophotometer (NanoDrop Technologies Inc., Wilmington, DE, USA) was employed. Only high-quality RNA samples (optical density [OD] 260/280 = 1.8–2.2, OD 260/230 $\geq$ 2.0, RNA integrity number $\geq$ 6.5, 28S:18S $\geq$ 1.0, $>$1 µg) were deemed suitable for the subsequent construction of sequencing libraries.

RNA purification, coupled with reverse transcription, library assembly, and ultimately sequencing, were conducted in accordance with the instructions of the manufacturer (Illumina, San Diego, CA, USA). The Illumina Stranded mRNA Prep Ligation Kit was used to construct the RNA sequencing (RNA-seq) transcriptome library, which was accomplished with precise input of 1 µg total RNA, ensuring the highest degree of precision and conformity with academic rigor. Using oligo (dT) beads and polyA selection, mRNA was separated and fragmented using designated buffers. Double-stranded cDNA synthesis was achieved using the SuperScript III First-Strand Synthesis System (Invitrogen, Carlsbad, CA, USA) and random hexamer primers (Illumina). The cDNA was subjected to phosphorylation, 'A' tailing, and end repair in accordance with Illumina's methodology, enhancing its suitability for library construction. The cDNA (300 bp) was separated on a 2% ultra-agarose gel (Thermo Fisher Scientific, Waltham, MA, USA), followed by PCR amplification utilizing phusion DNA polymerase (New England Biolabs, Ipwich, MA, USA) for 15 cycles. Subsequently, the paired-end RNA-seq library was quantified with Qubit 4.0 (Thermo Fisher Scientific, Waltham, MA, USA) and sequenced on the advanced NovaSeq X Plus platform (Illumina). The initial paired-end sequencing data were trimmed and Fastp was adopted for quality control [20], utilizing its standard parameter settings. Next, using HISAT2 v2.2.1 (Daehwan Kim Lab, Johns Hopkins University, Baltimore, MD, USA), clean reads were separately aligned to the reference genome in orientation mode [21]. The StringTie reference-based transcriptome assembler was used to assemble each sample's mapped readings [22].

2.7 Differential Expression Analysis and Functional Enrichment

To detect differentially expressed genes (DEGs) between different samples, transcripts per million methodology was used to assess transcript abundance. RNA-Seq by Expectation-Maximization was employed for quantitative gene expression profiling [23]. DESeq2 or DEGseq was used for differential expression analysis [24,25]. DEGs were considered significantly differentially expressed if they had |log2FC| $\geq$ 1 and false discovery rate (FDR) $\leq$ 0.05 (DESeq2) or FDR $<$ 0.001 (DEGseq). The study employed functional enrichment analysis, utilizing Gene Ontology (GO) and Kyoto Encyclopedia of Genes and Genomes (KEGG) to determine the DEGs that had high enrichment in GO terms and metabolic pathways. These analyses were conducted with stringent statistical thresholds, applying a Bonferroni-corrected $p \leq 0.05$ against the entire transcriptome as a backdrop. Specifically, GO annotations were enriched using GOATools, while KEGG pathway analyses were conducted with KEGG Orthology-Based Annotation System software (KOBAS 3.0, Peking University, Beijing, China) [26].

2.8 Weighted Gene Co-expression Network Analysis

To investigate the co-expression network in our cohort, we conducted intricate analysis leveraging the weighted gene co-expression network analysis (WGCNA) framework. Utilizing comprehensive transcriptomic profiles derived from HLECs, we conducted methodical identification of the optimal soft-thresholding parameter, harnessing the pickSoftThreshold functionality within the WGCNA package 1.71. This step ensures adherence to the stringent scale-free topology principle, which is fundamental for constructing robust networks. Subsequently, we computed the adjacency matrix and converted it into the topological overlap matrix (TOM). Employing this refined TOM, we quantified dissimilarity metrics pivotal for hierarchical clustering. To identify distinct, biologically meaningful gene modules exhibiting coordinated expression patterns, we applied the dynamic tree cutting algorithm, implementing a threshold of a minimum module size of 30. To establish the relevance of these gene modules to our study, we assessed the gene significance values and module membership values. This approach enabled us to pinpoint key modules associated with our experimental variables, thereby shedding light on the intricate molecular machinery underlying the phenotypic alterations observed in LECs.

2.9 Construction of A Protein–protein Interaction Network

We performed protein–protein interaction (PPI) analyses of DEGs focusing on the phosphoinositide 3-kinase/AKT pathway using the Search Tool for the Retrieval of Interacting Genes/Proteins (STRING) database (https://string-db.org/) with a confidence score threshold of $\geq$ 0.4. The key nodes and interactions were analyzed to highlight the role of LPAR1 in the pathway.

2.10 Quantitative PCR (qPCR)

cDNA synthesis employed the PrimeScript RT Reagent Kit sourced from Takara, Japan. qPCR analysis was conducted on the ABI 7500 Real-Time PCR System (Applied Biosystems, Waltham, MA, USA), utilizing SYBR Premix Ex Taq (Takara, Japan). The levels of

expression for LPAR1 and mammalian target of rapamycin (mTOR) were quantified using the $2^{-\Delta\Delta Ct}$ method, normalizing to GAPDH as a reference point internally. The primers specific to these genes were procured from Sangon Biotech, Shanghai, China. Three independent repeat experiments were conducted.

2.11 Molecular Docking

The crystal structure of the LPAR1 protein (PDB ID: 7YU4) was obtained from the RCSB PDB database (https://www.rcsb.org/). PyMOL software (version 2.x, Schrödinger, LLC, New York, NY, USA) was used for initial processing, where solvent molecules and small ligands were removed. The protein structure was further processed using ADFRsuite-1.0 (Scripps Research, La Jolla, CA, USA), retaining its native charges, and was converted into the pdbqt format for docking. For the ligand, the small molecule structure of dexamethasone was downloaded from the PubChem database. Similar preprocessing steps were performed using ADFRsuite-1.0 to retain charges and convert it into pdbqt format.

The docking process was carried out using AutoDock Vina 1.2.5 (The Scripps Research Institute, La Jolla, CA, USA). The docking grid for LPAR1 was centered at the coordinates (center_x = 165.337, center_y = 151.376, center_z = 152.603), with a box size of (size_x = 64.36 Å, size_y = 44.56 Å, size_z = 50.91 Å). A grid spacing of 0.375 Å and an exhaustiveness parameter of 32 were used. The prepared pdbqt files of LPAR1 and dexamethasone were input into AutoDock Vina, and docking was executed with these parameters. The resulting docking conformations were ranked by binding energy, and the best-scoring pose was selected for analysis.

2.12 Data Analyses

This sample size was determined based on our preliminary experimental data and sample size calculation, aiming to achieve a statistical power of 0.8 at a 0.05 significance level. We used SPSS 29.0.2 (IBM Corporation, Armonk, New York, NJ, USA) to conduct statistical analysis and created the statistical graphs by using GraphPad Prism software, version 10.2.2. Depending on the dexamethasone concentration, cells were categorized into 0 µM, 0.25 µM, and 0.5 µM groups. Variables in each group followed a normal distribution, tested by Shapiro-Wilk. For comparison of variables among the three groups, one-way ANOVA was used and test for homogeneity of variance were first performed. The nuclear area of HLE-B3 cells satisfied variance alignment among the groups and further post hoc comparisons were made using Tukey's test. The groups of HLE-B3 cell length, cell area, cytoplasmic area, and nuclear-cytoplasmic ratio did not satisfy variance alignment, and then corrected for this using Welch's test with a Tamhane T2 test for post hoc comparison. For direct comparisons between pairs, the student's t-test was adopted. The comparison of FSC and SSC between the control group and the 0.25 µM dexamethasone group was performed using a t-test, as the data followed a normal distribution and had equal variances. For the PCR experiment, the mRNA expression levels between the control group and the 0.25 µM dexamethasone group were also analyzed using a t-test, with the data meeting the assumptions of normal distribution and equal variances. The average fluorescence intensity of LPAR1 in immunofluorescence staining between the control group and the 0.25 µM dexamethasone group was calculated using a t-test, with the data normally distributed and variances equal. However, for the average fluorescence intensity of S6K1 in immunofluorescence staining between the control group and the 0.25 µM dexamethasone group, where the variances were unequal, Welch's correction was applied. $p < 0.05$ was considered statistically significant. The results are shown as the mean ± standard deviation (SD). Additionally, transcriptome datasets underwent rigorous bioinformatic analysis to identify DEGs and potential signaling cascades. In this study, no missing values were found in the dataset.

3. Results

3.1 Dexamethasone Treatment Leads to An Increase in The Area of HLECs

The concentration of dexamethasone in the blood that leads to GC-induced cataracts is 0.15 µmol/L, with this level of exposure typically occurring over a period of 2 years [27,28]. A previous study has shown that low-dose dexamethasone (0.1 µM) leads to increased proliferation of HLECs, while exposure to dexamethasone concentrations above 1 µM results in the apoptosis of HLECs [29]. Therefore, we chose 0.25 µM and 0.5 µM concentrations based on their relevance to physiological conditions and clinical scenarios.

We cultured HLE-B3 cells *in vitro* and treated them with different concentrations of dexamethasone (0, 0.25, and 0.5 µM). To analyze the expression of specific proteins and intermediate filament proteins in HLE-B3 cells, we performed immunofluorescence staining for α-crystallin, γ-crystallin, and vimentin, and found that they were widely expressed in HLE-B3 cells, with strong fluorescent signals observed in the cytoplasm (Fig. 2B). α-crystallin and γ-crystallin are specific to the lens and crucial for its transparency, whereas vimentin supports cell structure and function. The detection of α-crystallin, γ-crystallin, and vimentin proteins via immunofluorescence staining in HLE-B3 cells confirmed their identity as LECs and ensured the reliability of the experimental results on the effects of dexamethasone on HLECs. The cultured cells under a phase-contrast microscope are shown in Fig. 2A.

The cell length, cell area, nuclear area, cytoplasmic area, and nuclear-cytoplasmic ratio after 60 days of cell culture are expressed as the mean ± SD. One-way ANOVA was used to compare these results among the three groups

(**Supplementary Table 1**). Furthermore, for variables that satisfy variance alignment and those that do not, we use Tukey's test and Tamhane T2 test for post hoc comparisons respectively (**Supplementary Table 2**). The results showed that the 0.25 and 0.5 μM dexamethasone-treated groups showed an increase in cell length, cell area, and cytoplasmic area, and a decrease in nuclear-cytoplasmic ratio (Fig. 2C–G).

We further analyzed the cell size and intracellular granularity of the control group and 0.25 μM dexamethasone group using flow cytometry. We used the parametric Student's t-test to compare the cell size and intracellular granularity between the control group and 0.25 μM dexamethasone group. Flow cytometry results indicated that the average cell size was greater in the 0.25 μM group than in the control group (t = 3.528, p = 0.0243; Fig. 3A,B), and there was an increase in cell granularity (t = 24.41, $p <$ 0.001; Fig. 3C,D). Increased granularity within LECs may indicate changes in autophagic activity, cellular stress responses, or the aggregation of crystalline [30,31]. It has been shown that in GIC in $vivo$, the proliferation of LECs is abnormally regulated and differentiated, producing modest amounts of extracellular granular and fibrillar material as well as increased cell area [32,33]. Previous studies have indicated that in patients with GIC, the lens fiber cells contain nuclei and organelles, which lead to an increase in intracellular granularity [34,35]. The results of the experiments showed that dexamethasone treatment resulted in increased cell length and area and increased granularity in HLECs in $vitro$. This phenomenon may affect the processes of cell proliferation and differentiation and inhibit autophagy by regulating mammalian target of rapamycin (mTOR) activity. The results of the in $vitro$ experiments were similar to the morphological changes observed in HLECs in GIC in $vivo$.

3.2 High-throughput Transcriptome Sequencing to Investigate Pathways Affected by Dexamethasone in HLECs

To investigate the specific mechanisms by which dexamethasone affects the morphology and function of HLECs, we performed high-throughput transcriptome sequencing on the control, 0.25, and 0.5 μM groups. Analysis of DEGs suggested that there was only one DEG between the 0.25 and 0.5 μM dexamethasone groups (Fig. 4A,B). Therefore, we subsequently chose to compare the control group and 0.25 μM dexamethasone group for further analyses.

Using a corrected $p <$ 0.05 and fold change ≥ 2 as selection criteria, 427 genes were greatly downregulated and 443 genes were greatly upregulated in the 0.25 mmol/L dexamethasone group compared with the control group (Fig. 4C). Remarkable differences in mRNA expression between the control group and 0.25 μM dexamethasone group were observed, as shown in the heatmap in

Fig. 4D. To further investigate the effects of dexamethasone on HLECs, GO enrichment analysis was conducted. The results showed that the DEGs are closely linked to the steroid hormone response, response to GC, regulation of smooth muscle contraction, response to growth factors, regionalization, and positive regulation of cell–cell adhesion (Fig. 5A,C). KEGG enrichment analysis identified pathways related to human diseases, environmental information processing, and cellular processes such as rheumatoid arthritis, malaria, interleukin 17 signaling pathway, cancer signaling pathways, calcium signaling pathway, PI3K/AKT signaling pathway, and tumor necrosis factor signaling pathway, among others (Fig. 5B,D). These enriched pathways further confirmed the accuracy of high-throughput transcriptome sequencing and its similarity to in $vivo$ experiments.

3.3 Transcriptome Sequencing Analysis of the Effects of Dexamethasone on HLECs

We identified the top 20 pathways related to the morphological and biological effects of dexamethasone on HLECs using KEGG and GO analyses. Genes within these pathways were compiled into a gene set (**Supplementary Table 3**). WGCNA analysis was conducted to identify gene modules and central genes within the group. We established a scale-free co-expression network with a soft threshold of 9 and a scale-free index of –0.095, demonstrating good mean connectivity (Fig. 6A,B). The clustering dendrogram is depicted in Fig. 6C, and the genes were ultimately clustered into two modules (Fig. 6D).

We calculated the correlation between the two modules and the effects of dexamethasone on the size of HLECs. The module significance analysis indicated that the MEblue module was the most significant (Fig. 6E). The MEblue module included 56 genes and was considered important in the effects of dexamethasone on cell size. A network visualization of genes within the MEblue module showed key gene interactions (Fig. 7A). Hub genes identified in this module included atypical chemokine receptor 1, secreted frizzled related protein 1, collagen type IV alpha 4 chain, LPAR1, and growth arrest specific 1, which may play crucial roles in the effects of dexamethasone on cell size. Among these, LPAR1, a subtype of GPCRs, has not been previously reported to interact with dexamethasone and affect cell morphology and function. LPAR1 activates the PI3K/AKT pathway, one of the top 20 KEGG enriched pathways, and is associated with the "response to organophosphorus" term in the top 20 GO enriched pathways. To understand the interactions between LPAR1 and other proteins in the PI3K/AKT pathway, we screened the top 20 KEGG enriched pathways of DEGs, focusing on genes in the PI3K/AKT pathway, and constructed a PPI network diagram using the STRING database (Fig. 7B).

Moreover, high-throughput transcriptome sequencing revealed differentially expressed autophagy-related genes,
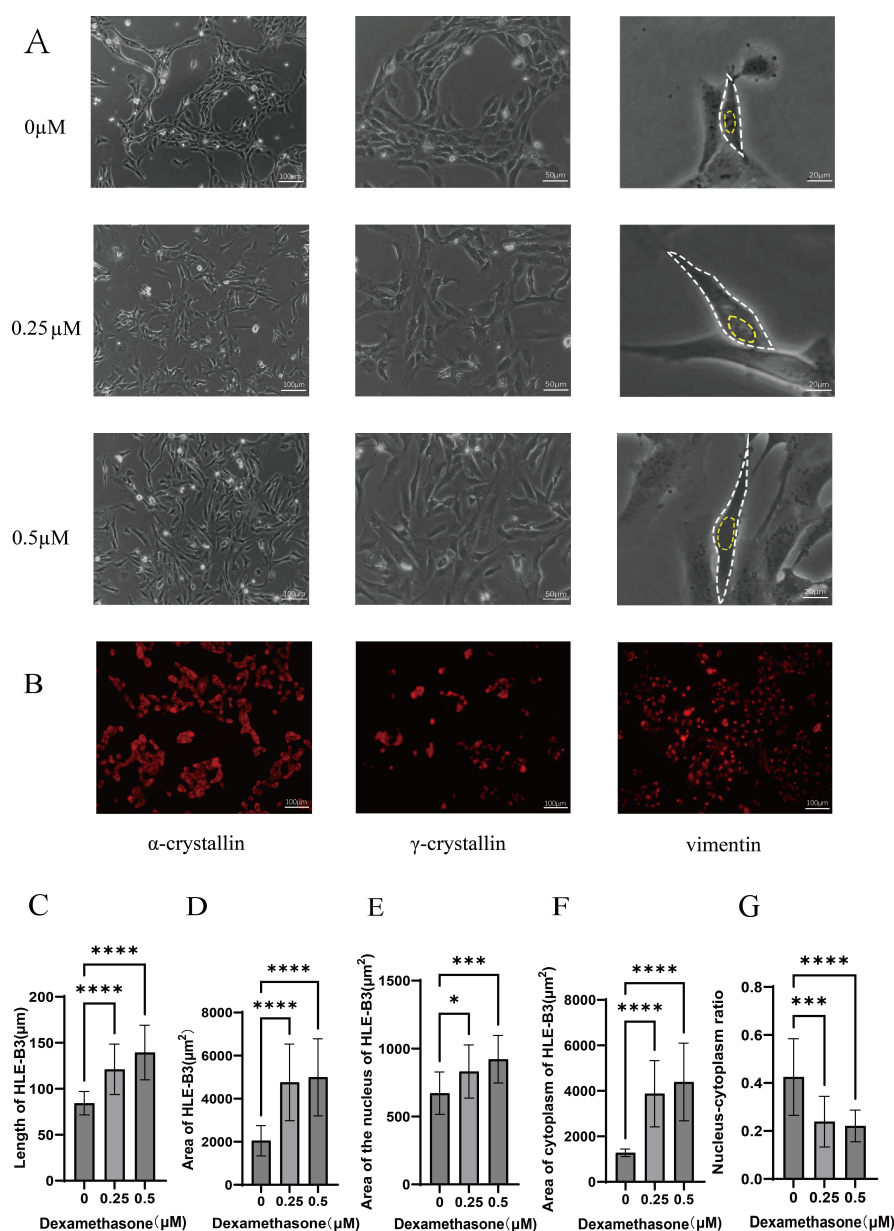
Fig. 2. Morphologic effects of different concentrations of dexamethasone on HLE-B3 cells and immunofluorescence staining of HLE-B3 cells. (A) The morphology of HLE-B3 cells is shown for the 0, 0.25, and 0.5 µM groups. The white circles represent the cell contours, whereas the yellow circles represent the cell nuclei. Scale bars represent 100 µm for the first column, 50 µm for the second column, and 20 µm for the third column, respectively. (B) Immunofluorescence staining of HLE-B3 cells for α-crystallin, γ-crystallin, and vimentin. Scale bar = 100 µm. (C) Analysis of cell length among the control, 0.25, and 0.50 µM groups (n = 30). (D) Analysis of cell area among the control, 0.25, and 0.50 µM groups (n = 20). (E) Analysis of the nuclear area among the control group, 0.25, and 0.50 µM groups (n = 20). (F) Analysis of the cytoplasmic area among the control, 0.25, and 0.50 µM groups (n = 20). (G) Analysis of the nuclear-cytoplasmic ratio among the control, 0.25, and 0.50 µM groups (n = 20). The data are shown as the mean $\pm$ SD. All variables follow a normal distribution. The data of the cytoplasmic area among the control, 0.25, and 0.50 µM groups meet the assumption of homogeneity of variance, whereas other data do not. p-values were obtained by ANOVA single factor analysis and are shown in the graphs (* <0.05; *** <0.001; **** <0.0001).

such as DDIT4, RPS6KA2, and IRS1 (**Supplementary Table 4**). KEGG enrichment analysis of these DEGs also indicated the involvement of key autophagy-related pathways, including mTOR, PI3K/AKT, and AMPK signaling.

Based on the changes in the PI3K/AKT signaling pathway indicated by KEGG and GO analyses, we speculate that dexamethasone interacts with LPAR1, triggering a series of signaling responses that affect the PI3K/AKT/mTOR
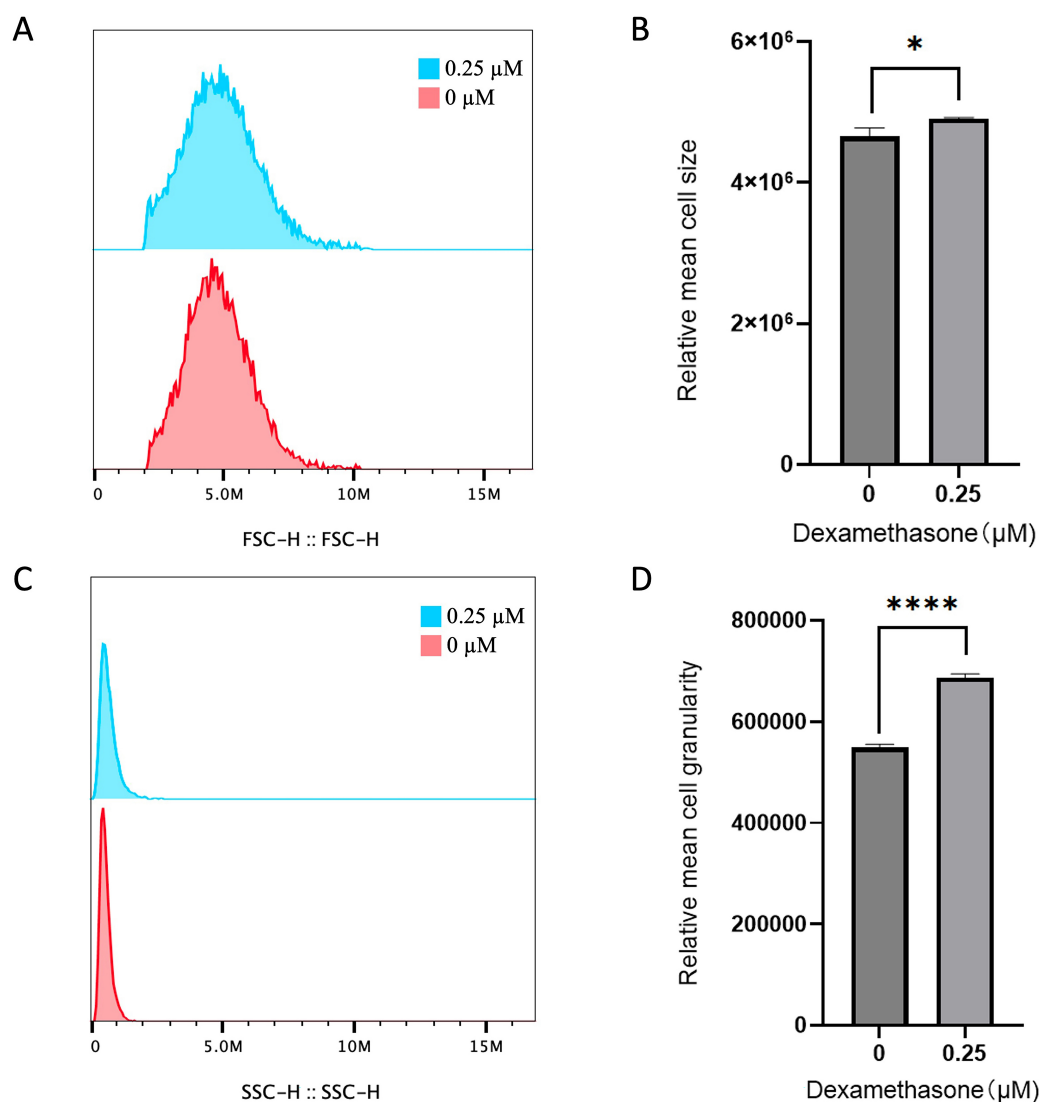
Fig. 3. Dexamethasone increases HLE-B3 cell size and granularity. (A) The relative sizes of HLE-B3 cells were compared by measuring forward scatter (FSC) values through fluorescence-activated cell sorting analysis. (B) The mean sizes of HLE-B3 cells were obtained and are shown in a graph (n = 3). (C) The relative cell granularity of HLE-B3 cells was compared using side scatter (SSC) analysis. (D) The mean granularity of the HLE-B3 cells was obtained and are shown in a graph (n = 3). The data are shown as the mean $\pm$ SD. p-values were obtained by the parametric Student's t-test and are shown in the graphs (* <0.05; **** <0.0001).

pathway. These effects, in turn, lead to increased LEC length, enhanced crystallin protein synthesis, and autophagy inhibition.

3.4 Further Evidence Suggests that LPAR1 Interacts with Glucocorticoids, Impacting the PI3K-AKT-mTOR Pathway

We have conducted PCR validation, which showed significantly increased expression of LPAR1 and mTOR in the 0.25 μM dexamethasone group (t = 9.158, $p < 0.001$; t = 59.854, $p < 0.001$; Fig. 8A). Additionally, we performed immunofluorescence staining to assess the LPAR1 and the phosphorylation of ribosomal protein S6 kinase beta-1 (S6K1), which is a key downstream effector of the mTOR signaling pathway (Fig. 8B,D). Quantification using ImageJ revealed higher immunofluorescence intensities for LPAR1 and phosphorylated S6K1 in the 0.25 μM dexamethasone group (t = 5.085, $p = 0.007$; t = 3.061, $p = 0.038$; Fig. 8C,E).

In addition, we have performed molecular docking between LPAR1 and dexamethasone shown in Fig. 9, and the results suggest that the binding between the LPAR1 protein and dexamethasone molecule is spontaneous, with a relatively high affinity (binding energy of –8.16 kcal/mol). Interaction analysis revealed multiple types of interactions, including one salt bridge, one electrostatic interaction, four hydrogen bonds, one halogen bond, and six hydrophobic interactions. Key residues involved in these interactions
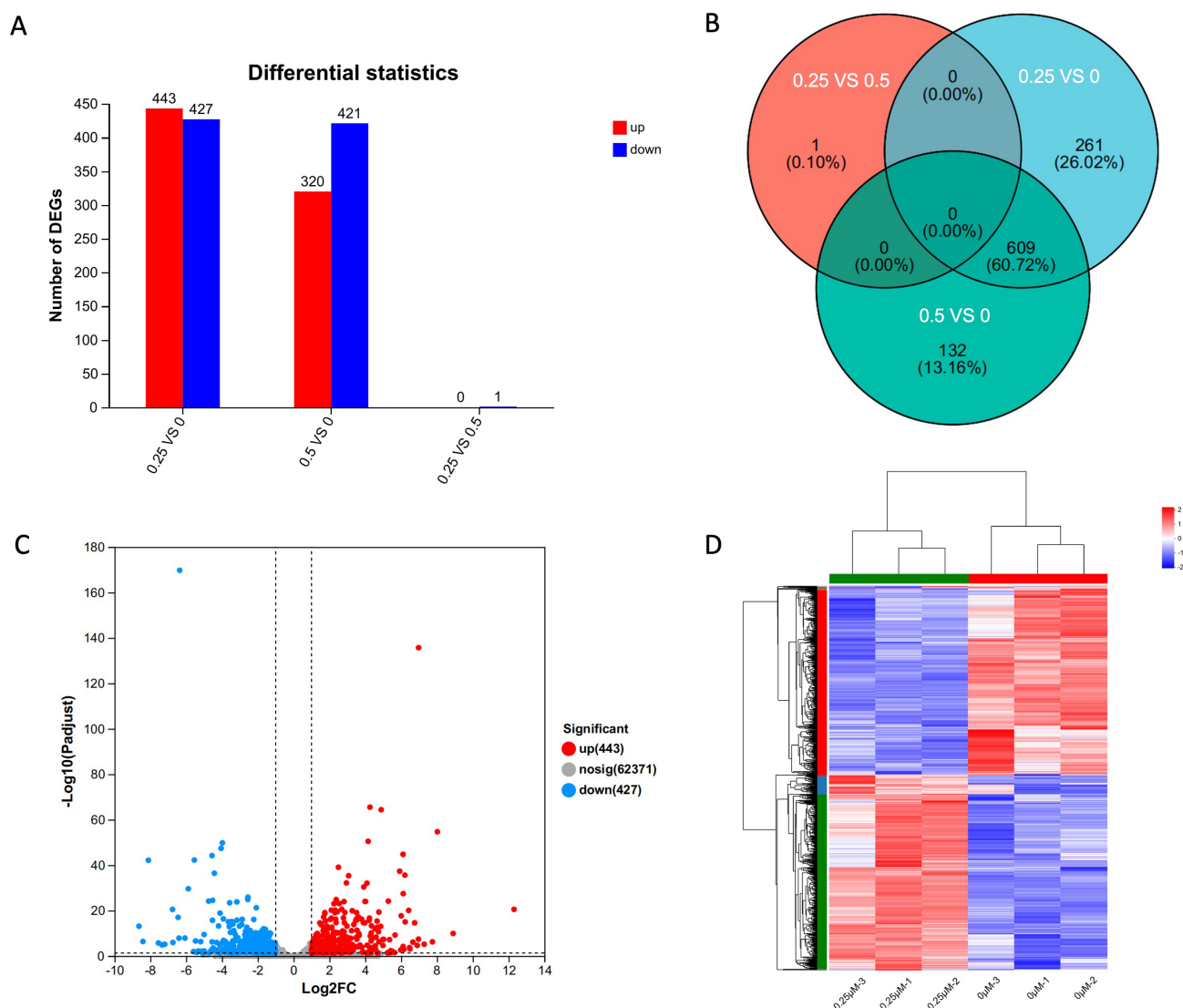
Fig. 4. Differential gene expression analysis in HLE-B3 cells treated with dexamethasone. (A) Statistical chart of DEGs between groups. (B) Venn diagram of DEGs between groups. (C) Volcano plot showing the changes in HLE-B3 genes in the 0.25 µmol/L dexamethasone group (fold change ≥2). (D) The heatmap displays gene expression across different groups of DEGs. Colors on the heatmap represent normalized gene expression levels, ranging from high (red) to low (blue). DEGs, Differentially expressed genes.

were LYS294 (salt bridge), LYS39 (electrostatic interaction), GLU293, LYS39, and GLN125 (hydrogen bonds), and several leucine residues contributing to hydrophobic interactions. These interactions significantly stabilize the binding of dexamethasone to LPAR1.

These results further provide molecular-level evidence to back the mechanistic claim that LPAR1 interacts with glucocorticoids, impacting the PI3K-AKT-mTOR pathway (Fig. 10), which in turn affects the morphology, area, and autophagic functions of LECs.

4. Discussion

LECs play an important role in maintaining the transparency of lens. It has been demonstrated that dexamethasone can affect the morphology and function of LECs,

which in turn leads to the development of GIC [36,37]. However, the specific molecular mechanism remains unclear. In the current study, we demonstrated *in vitro* that dexamethasone increases the length, area, and granularity of HLECs and inhibits autophagy, thereby affecting their biological functions.

Flow cytometry (FCM) is a sophisticated method that utilizes light scattering and fluorescence emission principles as cells tagged with fluorescent probes move through a laser beam. When a laser beam is directed at a cell, the excitation light is scattered in both the forward and lateral directions. FSC reflects cell size, SSC reflects intracellular granularity. It enables fast, relatively quantitative multi-parameter analysis of cell populations at the single-cell level. Cell size, the integrity of the membrane, and the

GO enrichment analysis

KEGG enrichment analysis

GO term

KEGG Pathway
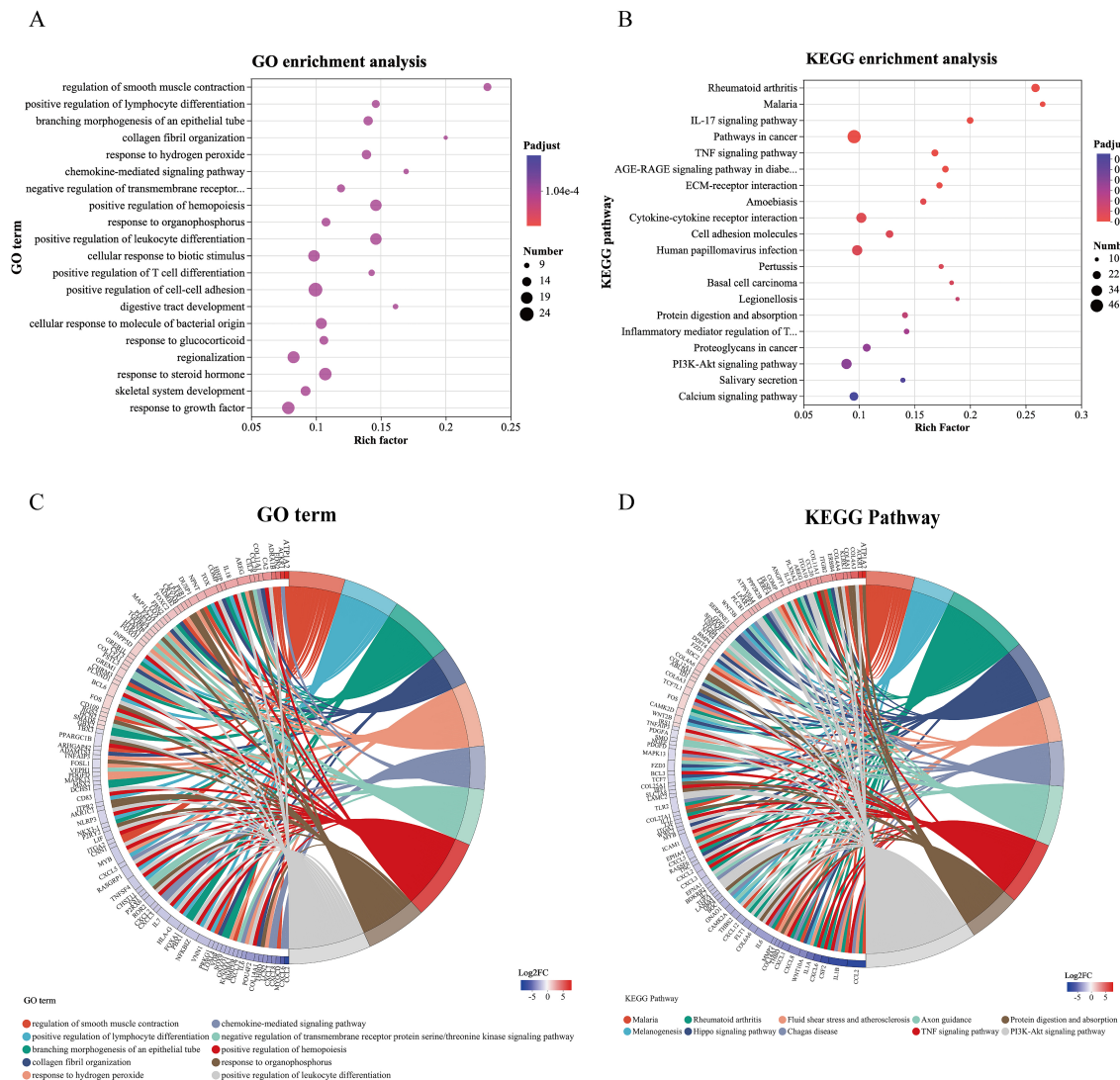
Fig. 5. GO and KEGG enrichment analyses. (A) Bubble plot illustrating the GO enrichment analysis between the control group and 0.25 µmol/L dexamethasone group. The x-axis represents the rich factor, whereas the y-axis lists the GO terms. The bubble size indicates the number of genes, and the bubble color corresponds to the adjusted *p*-value (*p*adjust). (B) Bubble plot illustrating KEGG pathway enrichment analysis between the control group and the 0.25 mmol/L dexamethasone group. The x-axis represents the rich factor, whereas the y-axis lists the KEGG pathways. The bubble size indicates the number of genes, and the bubble color corresponds to the *p*adjust. (C) Enriched chordal diagram showing the relationships between the DEGs and enriched GO terms. The different colors represent various GO terms. (D) Enriched chordal diagram showing the relationships between DEGs and enriched KEGG terms. Different colors represent various KEGG terms. DEGs, Differentially expressed genes; GO, Gene Ontology; KEGG, Kyoto Encyclopedia of Genes and Genomes.

relative quantity of biomolecules are among the properties of cells that are frequently examined. Using this technique, up to 70,000 cells can be detected per second [38]. Phase contrast microscopy is not as efficient and does not allow for observation of granularity, so we use flow cytometry as a complement to quantitative analysis of cell morphology. The results showed that dexamethasone resulted in increased cell size and increased granularity in HLECs. Our research indicates that a certain concentration of dexamethasone leads to an increase in the size of LECs, resulting in a decrease in cell density. This reduction in the number

of cells functioning as Na^+/K^+-ATPase and Ca^{2+}-ATPase may impair the overall ion-pumping capacity of the lens epithelium, thereby affecting ion metabolism within the lens and leading to cataract [39,40]. Additionally, LECs synthesize cholesterol, an essential component of the cell membrane that helps maintain low oxygen pressure, which is crucial for preserving lens transparency [41]. A decrease in the density of LECs may reduce cholesterol synthesis, potentially contributing to cataract [42].

A large number of previous studies have been done on lens epithelial cells using different methods with the aim of
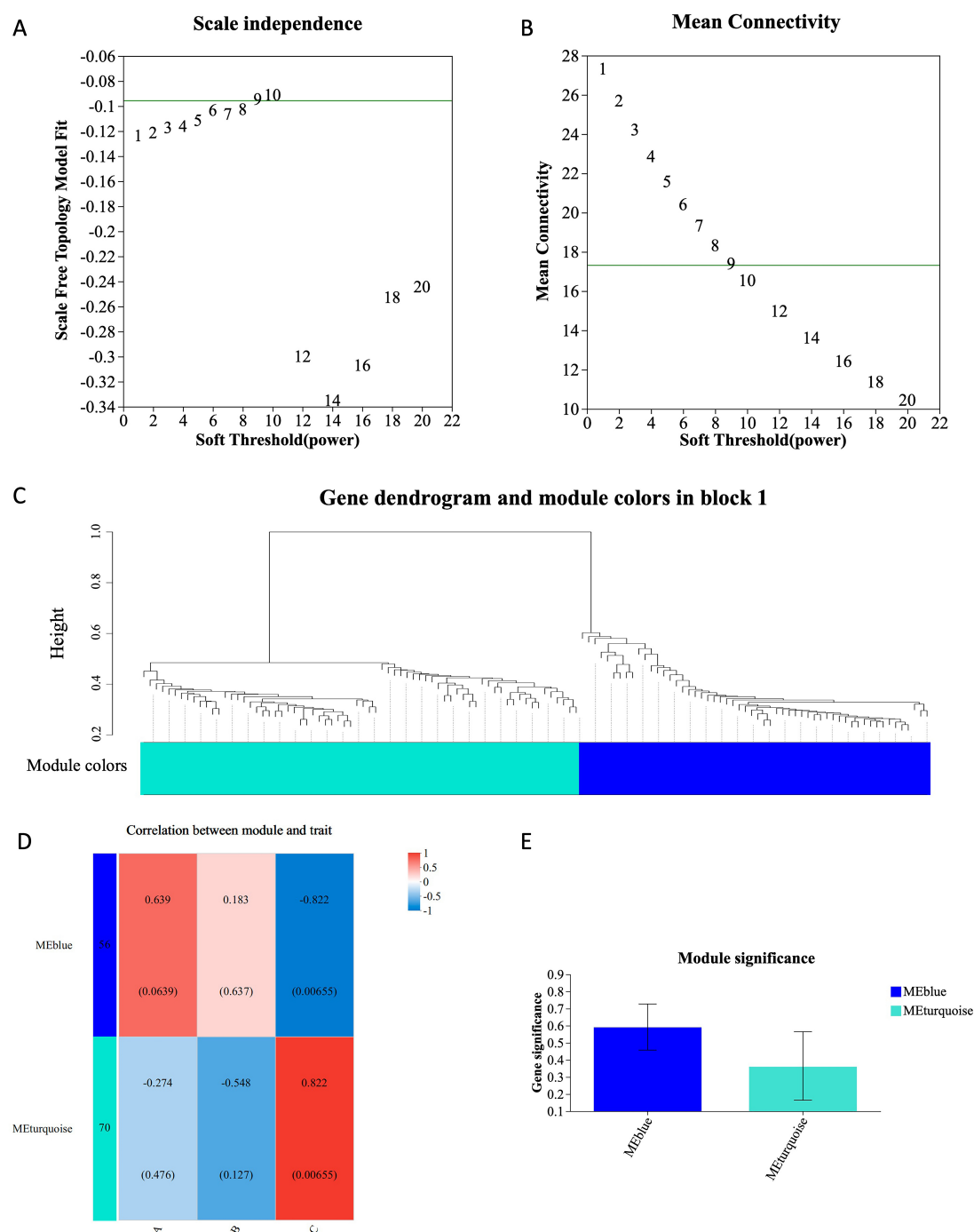
Fig. 6. WGCNA analysis and discovery of potential hub genes. (A) Soft threshold power of WGCNA. (B) Mean connectivity of WGCNA. (C) WGCNA cluster dendrogram. (D) WGCNA clustered modules. (E) Analysis of module significance. WGCNA, Weighted gene co-expression network analysis.

identifying potential pathways that affect their normal morphology and function. A study performed proteomic analysis of HLEC line (SRA01/04) after ultraviolet B irradiation to investigate the relationship between lens ubiquitination and the development of age-related cataracts (ARC) [43]. Gong *et al*. [44] used lipidomics to study metabolic differences in LECs in patients with ARC of varying severity, and pathway analysis showed that glycerophospholipid metabolism was significantly affected. Additionally, other studies have used microarray analysis to identify genes and transcription factors related to the effects of GCs on HLECs. These studies showed that GCs can regulate the PI3K/AKT signaling pathway, downregulate the expression of C-C motif chemokine ligand 2, and upregulate the expression of dual specificity phosphatase 1 and FAS cell surface death receptor [45–47]. However, the number of
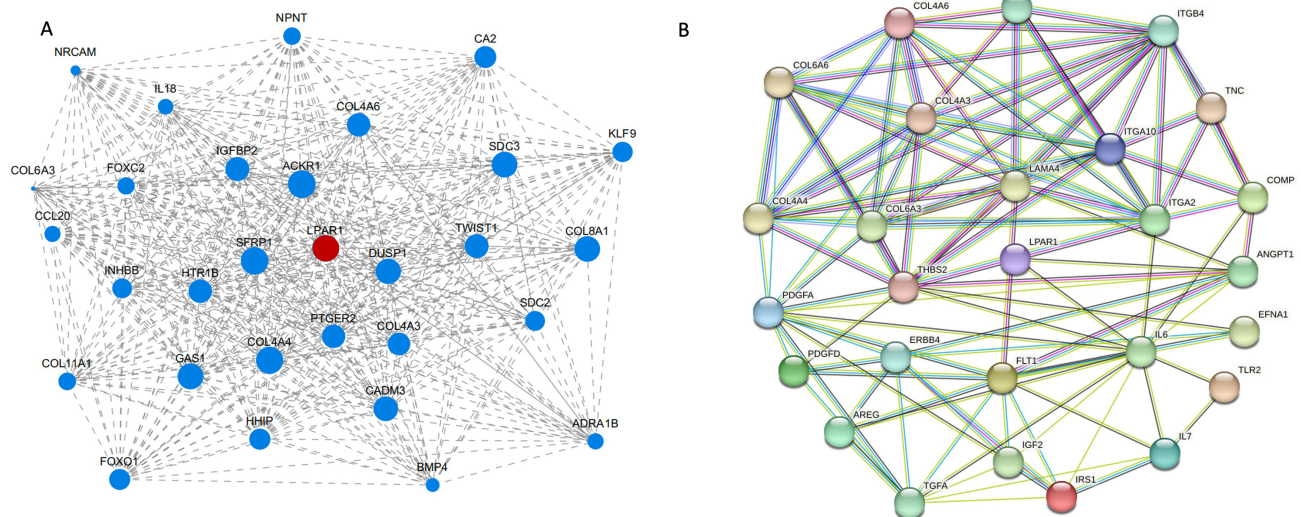
Fig. 7. Recognition of hub genes and the protein–protein interaction network. (A) Network display of key genes. (B) Each node represents a protein, and the lines represent an association between proteins. COL4A6, Collagen Type IV Alpha 6 Chain; COL6A6, Collagen Type VI Alpha 6 Chain; COL4A4, Collagen Type IV Alpha 4 Chain; COL4A3, Collagen Type IV Alpha 3 Chain; COL6A3, Collagen Type VI Alpha 3 Chain; LAMC2, Laminin Subunit Gamma 2; LAMA4, Laminin Subunit Alpha 4; ITGB4, Integrin Beta 4; ITGA10, Integrin Alpha 10; ITGA2, Integrin Alpha 2; TNC, Tenascin C; COMP, Cartilage Oligomeric Matrix Protein; LPAR1, Lysophosphatidic Acid Receptor 1; THBS2, Thrombospondin 2; PDGA, Platelet-Derived Growth Factor Alpha; PDGFD, Platelet-Derived Growth Factor D; ERBB4, Erb-B2 Receptor Tyrosine Kinase 4; ANGPT1, Angiopoietin 1; AREG, Amphiregulin; FLT1, Fms Related Tyrosine Kinase 1; IL6, Interleukin 6; EFNA1, Ephrin A1; TGFA, Transforming Growth Factor Alpha; IGF2, Insulin-Like Growth Factor 2; IRS1, Insulin Receptor Substrate 1; IL7, Interleukin 7; TILR2, T cell immunoreceptor with Ig and ITIM domains 2.

detected genes by these methods are limited, and no studies have reported a role for LPAR1 and its mediated signaling pathways in GIC.

In the present study, we used high-throughput transcriptome sequencing to identify potential signaling pathways. High-throughput transcriptome sequencing, a second-generation sequencing technology, is based on the Illumina platform and sequences all mRNAs transcribed in a particular eukaryotic tissue or cell at a certain period of time [48]. Transcriptome sequencing directly analyses mRNA molecules, providing direct information about gene expression, whereas proteomics requires translation and modification before proteins can be detected, which can be affected by the state of the tissue and environment. Compared with the microarray approach, high-throughput transcriptome sequencing features high resolution to background interference and high sensitivity to low-expression genes, and is able to detect not only differential genes but also the expression abundance of related genes [49]. This study is the first to use a high-throughput sequencing approach to gain insights into the transcriptome changes in dexamethasone-treated HLECs [50].

G protein-coupled receptors (GPCRs) are the largest family of cell surface receptors in the human genome, with seven transmembrane helices of transmembrane protein receptors. Several studies have demonstrated the involvement of GPCRs in the pathogenesis of cataract. Frizzled

protein (FZD), an F-like GPCR, mediates the planar cell polarity pathway, which regulates directional cell migration and cellular polarization, such as lens epithelial differentiation and the highly ordered arrangement of fibroblasts, resulting in a variety of disorders, such as cataracts [51]. UV irradiation significantly increased the expression of let-7b in LECs, which promotes apoptosis through direct action on its target gene, G protein-coupled receptor 4 (Lgr4) [52]. What's more, Lgr4 deficiency impaired the resistance of rats' LECs to oxidative stress and accelerated the progression of age-related cataract [53]. Previously, researchers discovered a high-affinity membrane receptor for GCs, GPR97, and analyzed the structure of the complex between GPR97 and Go proteins under the activation of GCs by single-particle cryo-electron microscopy, which elucidated the structural basis for the binding and activation of the membrane receptor, GPR97, by GCs [16].

In the present study, our experimental results showed that the combination of dexamethasone and LPAR1 activates the downstream PI3K/AKT signaling pathway. LPAR1 is a GPCRs isoforms that are mediated by the second messenger pathway after coupling with G proteins Gi/0, Gαq, and G12/13 and are involved in the regulation of cell proliferation, migration, survival, apoptosis, and morphology. LPAR1 is present in a wide range of tissues of the human body, but is most abundantly expressed in the brain and plays an important role in a variety of cells of the
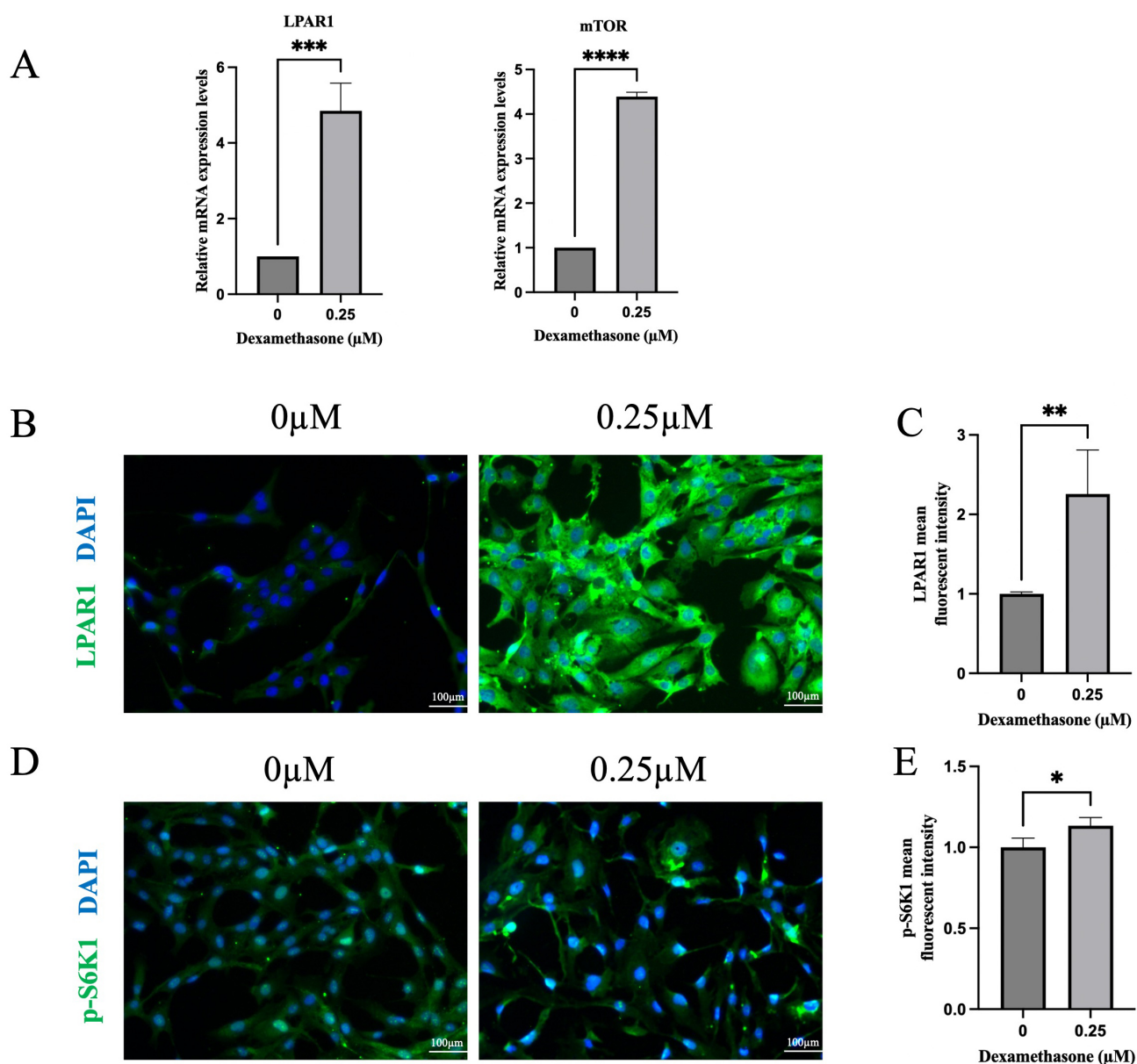
Fig. 8. Quantitative polymerase chain reaction (qPCR) and immunofluorescent staining of HLE-B3 cells with (0), 0.25 µM dexamethasone treatment. (A) qPCR analysis of the mRNA expression levels of *LPAR1* and *mTOR*. qPCR analysis is presented relative to the GAPDH expression data (n = 3). (B,C) Immunofluorescent staining of LPAR1 (green) merged with DAPI (blue) and relative fluorescence intensity of LPAR1 was quantified (n = 5). (D,E) Immunofluorescent staining of p-S6K1 (green) merged with DAPI (blue) and relative fluorescence intensity of p-S6K1 was quantified (n = 3). Data are shown as mean $\pm$ SD. p-values were obtained by the parametric Student's t-test and are shown in the graphs (* <0.05, ** <0.01; *** <0.001, **** <0.0001). Scale bar = 100 µm.

central nervous system, for example, its ability to regulate oligodendrocyte survival and apoptosis, morphology, and enhancement of oligodendrocyte differentiation and myelin formation [54]. In addition, it was found that LPAR1 is involved in several downstream molecular and signaling pathways together with the glucocorticoid receptor, including the PI3K/AKT pathway [55,56], the MAPK/ERK pathway and the RhoA signaling pathway [57–60]. These findings suggest that LPAR1 may act synergistically with the glucocorticoid receptor to co-regulate several cellular activ-

ities such as survival and proliferation, and that the interaction of these signaling pathways is critical for the maintenance of cellular functions.

As part of the GPCR superfamily, LPAR1 triggers the activation of the PI3K/AKT signaling pathway by interacting with Gαi/o proteins [17]. The PI3K/AKT pathway plays a crucial role in regulating various cellular processes such as proliferation, differentiation, viability, and metabolic functions [61–63], particularly plays a significant part in cataract development and progression, mainly
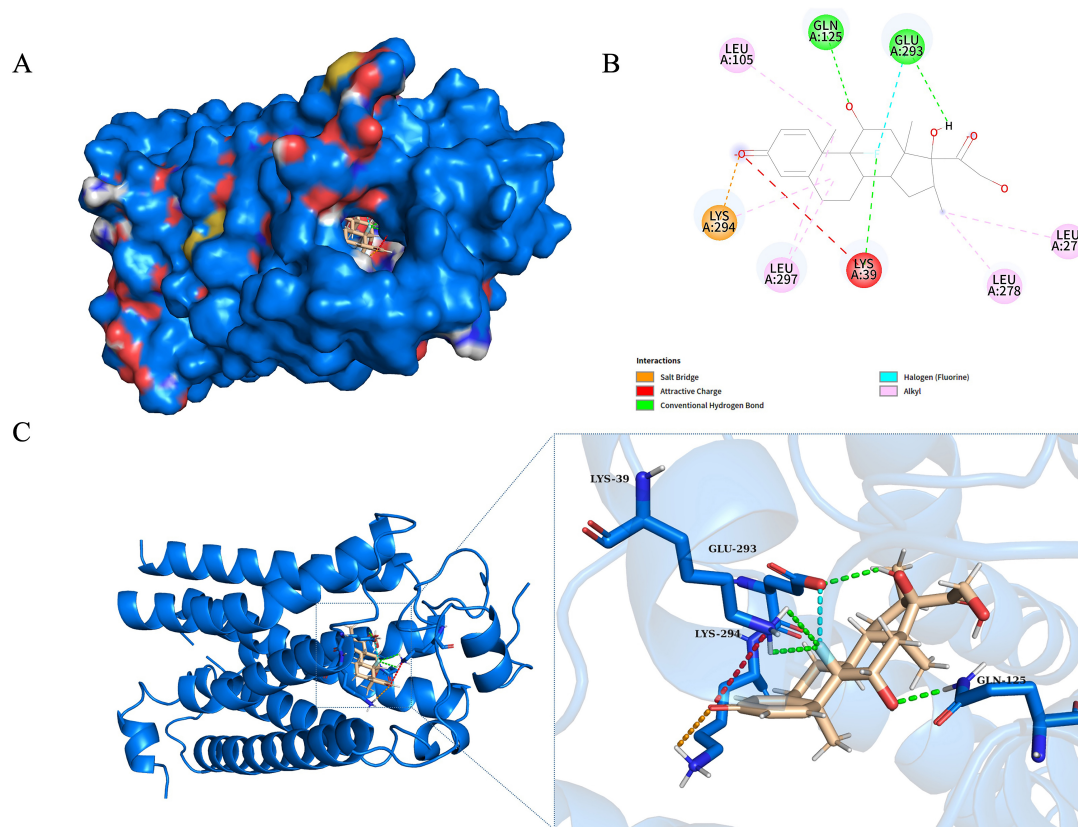
Fig. 9. Molecular docking results of LPAR1 protein with dexamethasone. (A) Surface representation of LPAR1 protein (blue) bound to dexamethasone (sticks in the binding pocket) illustrating the spatial fit and overall surface interactions. (B) 2D interaction diagram highlighting the key residues involved in the interaction between LPAR1 and dexamethasone. The diagram shows hydrogen bonds (green lines), attractive charge interactions (red lines), and salt bridges (orange lines). Involved residues include LYS39, LYS294, GLU293, GLN125, and several hydrophobic interactions (LEU105, LEU297, LEU278, and LEU277). (C) 3D cartoon representation of LPAR1 with a close-up of the binding pocket. The detailed view shows hydrogen bonding and electrostatic interactions between LPAR1 residues (blue sticks) and dexamethasone (beige sticks), with LYS39, GLU293, and LYS294 playing key roles.

in the regulation of LECs' proliferation, apoptosis, migration, and mesenchymal transition [64–66]. AKT further activates the downstream effector mTOR, a highly conserved serine/threonine kinase, acts as a key negative regulator of autophagy initiation. A previous study has shown that glucocorticoids disrupt intrinsic antimicrobial autophagy and promote Mycobacterium survival in macrophages through activation of the AKT-mTOR signaling pathway, making individuals highly susceptible to mycobacterial infection [67]. Autophagy is essential for maintaining the normal morphology and function of cells and tissues. It has previously been shown that autophagy is involved in the degradation of mitochondria and other organelles in lens epithelial and fiber cells [68]. When LECs fail to degrade damaged mitochondria via mitochondrial autophagy, they will not provide the cell with the energy it needs, leading to a loss of essential functions of lens enzymes and transport systems, as well as an increase in the production of reactive oxygen species, which oxidize and destabilize the lens, thus leading to the formation of cataracts [40]. Ma *et al.*

[69] found that high glucose levels inhibit autophagy via the mTOR signaling pathway, leading to diabetic cataracts. Therefore, we hypothesized that dexamethasone is involved in cataract development by affecting the proliferation and differentiation of HLECs and inhibiting autophagy through activation of the LPAR1-PI3K-AKT-mTOR signaling pathway, which was supported by the results of this study. This is the first report of dexamethasone interacting with LPAR1, suggesting that the effects of dexamethasone on LECs may be mediated through LPAR1, which provides a new theory and drug target for the prevention and treatment of GIC. Dexamethasone is a commonly used drug in clinical practice that can reduce ocular inflammation but is associated with cataract formation [70], this study may provide new ideas for reducing the incidence of adverse events in dexamethasone ophthalmic therapy.

The pathophysiologic mechanisms and potential therapeutic targets of GIC need to be explored in more depth. Currently, a few drugs targeting *LPAR1* have been researched and developed and have shown promising clinical
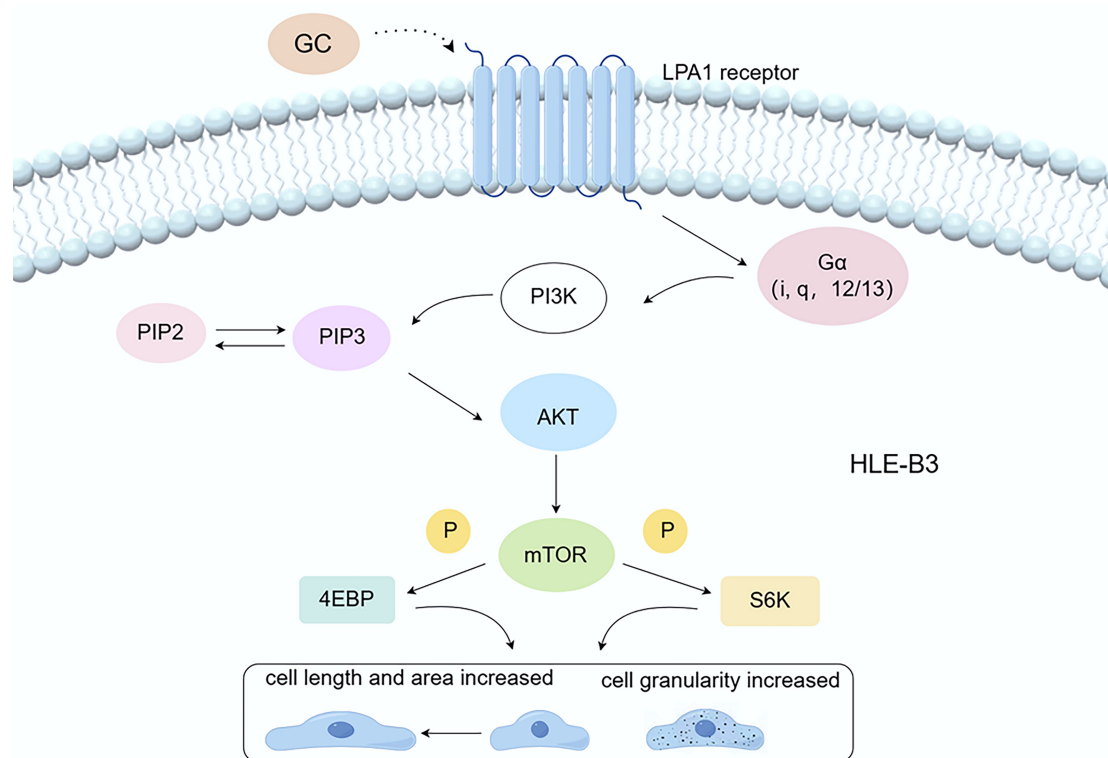
Fig. 10. The LPAR1/PI3K/AKT/mTOR pathway. Dexamethasone interacts with LPAR1, activating the PI3K/AKT/mTOR signaling pathway, which subsequently stimulates cell growth, increases cell size, and potentially enhances cell granularity relative to the group not treated with dexamethasone by inhibiting autophagy. GC, glucocorticoid; LPAR1, Lysophosphatidic acid receptor 1; PI3K, Phospho-inositide 3-kinase; PIP2, phosphatidylinositol-4,5-bisphosphate; PIP3, phosphatidylinositol-3 ,4,5-trisphosphate; AKT, protein kinase B; mTOR, Mammalian target of rapamycin; P, Phosphorylation; 4EBP, 4E-binding protein; S6K, p70 Ribosomal Protein S6 Kinase. By Figdraw (https://www.figdraw.com/#/).

significance. BMS-986278 is an *LPAR1* inhibitor for the treatment of pulmonary fibrosis and idiopathic pulmonary fibrosis. It has shown positive results in Phase 2 clinical trials, slowing the decline in lung function in patients with progressive pulmonary fibrosis [71]. In Addition, Ki-16425, an inhibitor of *LPAR1*, has been demonstrated to inhibit the proliferation of hepatocellular carcinoma (HCC) cells in a preclinical study [72]. By *LPAR1* inhibition, HCC cells can be induced to enter an oncogene-induced senescence state, thereby suppressing tumor growth [72]. We hypothesize that an *LPAR1* inhibitor could be developed in the future, perhaps in the form of an eye drop, to block the action of glucocorticoids on the HLECs and thus prevent GIC. Given the widespread use of glucocorticoids in the treatment of ocular inflammation and the study showing that ophthalmic preparations combining glucocorticoids with anti-infective drugs are effective in short-term therapy [73], treatment with dexamethasone in combination with an *LPAR1* inhibitor may reduce the risk of cataracts.

Future research could further explore the application of exosomes, nanomedicine, and RNA technologies in targeting *LPAR1* for the treatment of GIC. Nanomedicine, including nano micelles, nanoparticles, nanosuspensions, nano emulsions, microemulsions, nanofibers, dendrimers, liposomes, vesicles, nano wafers, contact lenses, hydrogels, microneedles, and other technologies, can serve as methods for ocular drug delivery [74]. Compared to traditional drug delivery methods, nanocarriers can overcome ocular barriers, enhance corneal permeability, prolong drug retention time, reduce drug degradation, lower dosing frequency, improve patient compliance, and achieve sustained/controlled release, drug targeting, and gene delivery [75]. Nanomaterial-mediated gene silencing is also a novel and promising approach for treating eye diseases [76]. Exosomes have been reported to treat ocular diseases with higher efficacy and fewer immune reactions [77], and targeting *LPAR1* through exosome delivery may enhance therapeutic outcomes. Moreover, therapeutic small interfering RNA (siRNA) can be loaded into exosomes via membrane fusion-mediated methods to exert therapeutic effects [78]. RNA technology could also be used to target the *LPAR1* gene for treatment. Intravitreal injection of lipid nanoparticles loaded with the circular RNA derived from the nerve growth factor gene has been shown to protect retinal ganglion cells and axons from degeneration caused by injury [79]. Additionally, a study has combined modified mRNA

technology with adipose-derived mesenchymal stem cell therapy, where IGF-1 modRNA (modIGF1)-engineered ADSCs (ADSC modIGF1) were applied to corneal alkali burns in mice, promoting corneal repair [80]. Additionally, we plan to conduct preliminary preclinical studies in large animal models, such as canines, non-human primates, and swine, to validate the potential of LPAR1 inhibitors. Following these studies, we will proceed with human clinical trials, particularly focusing on cataract patients who have long-term exposure to glucocorticoids. Further research are also needed to determine whether the effects of dexamethasone on HLECs involve other signaling pathways, such as those that inhibit autophagy [81] or organelle degradation [82], which may contribute to cataracts.

One limitation of our study is that while we have verified the involvement of the PI3K/AKT/mTOR pathway through PCR, immunofluorescence staining and molecular docking, we have not yet conducted knockdown experiments, such as *LPAR1* silencing, to fully confirm its role. To further address the functional validation of this interaction, we are planning to perform knockdown and inhibition of *LPAR1* in our future work. Future studies should include these functional assays to further clarify the effects of dexamethasone on HLECs and the specific pathways involved in GIC.

5. Conclusions

Certain concentrations of dexamethasone cause HLECs to elongate, increase in area, and change from a round to a spindle shape. Notably, the interaction between dexamethasone and LPAR1, a subtype of GPCRs, may modulate cell size and inhibit autophagy via the LPAR1/PI3K/AKT/mTOR pathway. These findings clarify the molecular mechanisms by which dexamethasone regulates lens function and contributes to GIC, thereby providing new molecular targets for the prevention and treatment of GIC.

Abbreviations

ARC, Age-related cataract; DEGs, Differentially expressed transcripts; FSC, Forward scatter; GCs, Glucocorticoids; GIC, Glucocorticoid-induced cataracts; GPCR, G protein-coupled receptor; GO, Gene Ontology; KEGG, Kyoto Encyclopedia of Genes and Genomes; LECs, Lens epithelial cells; LPAR1, Lysophosphatidic acid receptor 1; mTOR, mammalian target of rapamycin; PI3K, phosphoinositide 3-kinase; PPI, Protein–protein interaction; S6K1, Ribosomal protein S6 kinase beta-1; SSC, Side scatter; WGCNA, Weighted gene co-expression network analysis.

Availability of Data and Materials

All data from this study are available on reasonable request from the first author or the corresponding author.

Author Contributions

XS, YG, and JL designed the research study. XS and QL performed the research. XS, JG, and HX analyzed the data. XS, JG, and HX wrote the manuscript. JL and YG provided experimental funding and advice on the entire research process. All authors participated in the editorial revision of the manuscript. The final manuscript was read and approved by all authors. All authors have participated sufficiently in the work to take public responsibility for appropriate portions of the content and agreed to be accountable for all aspects of the work in ensuring that questions related to its accuracy or integrity.

Ethics Approval and Consent to Participate

This study was approved by the Ethics Committee of Chongqing Medical University Affiliated University Town Hospital, with the approval number LL-202364. All research procedures adhered to relevant laws and regulations.

Conflict of Interest

The authors declare no conflict of interest.

Supplementary Material

Supplementary material associated with this article can be found, in the online version, at https://doi.org/10.31083/j.fbl2911391.

References

[1] GBD 2019 Blindness and Vision Impairment Collaborators, Vision Loss Expert Group of the Global Burden of Disease Study. Causes of blindness and vision impairment in 2020 and trends over 30 years, and prevalence of avoidable blindness in relation to VISION 2020: the Right to Sight: an analysis for the Global Burden of Disease Study. The Lancet. Global Health. 2021; 9: e144–e160. https://doi.org/10.1016/S2214-109X(20)30489-7

[2] Hashemi H, Pakzad R, Yekta A, Aghamirsalim M, Pakbin M, Ramin S, *et al*. Global and regional prevalence of age-related cataract: a comprehensive systematic review and meta-analysis.

Eye (London, England). 2020; 34: 1357–1370. https://doi.org/10.1038/s41433-020-0806-3

[3] Shi Z, Zhao X, Su Y, Wang C, Liu P, Ge H. Screening of Biological Target Molecules Related to Glucocorticoid-Induced Cataract (GIC) on the Basis of Constructing ceRNA Network. Biochemical Genetics. 2022; 60: 24–38. https://doi.org/10.1007/s10528-021-10078-3

[4] Black RL, Oglesby RB, Von Sallmann L, Bunim JJ. Posterior subcapsular cataracts induced by corticosteroids in patients with rheumatoid arthritis. JAMA. 1960; 174: 166–171. https://doi.org/10.1001/jama.1960.63030020005014

[5] van den Brand FF, van der Veen KS, Lissenberg-Witte BI, de Boer YS, van Hoek B, Drenth JPH, et al. Adverse events related to low dose corticosteroids in autoimmune hepatitis. Alimentary Pharmacology & Therapeutics. 2019; 50: 1120–1126. https://doi.org/10.1111/apt.15528

[6] Nath T, Roy SS, Kumar H, Agrawal R, Kumar S, Satsangi SK. Prevalence of Steroid-Induced Cataract and Glaucoma in Chronic Obstructive Pulmonary Disease Patients Attending a Tertiary Care Center in India. Asia-Pacific Journal of Ophthalmology (Philadelphia, Pa.). 2017; 6: 28–32. https://doi.org/10.22608/APO.201616

[7] Thorne JE, Woreta FA, Dunn JP, Jabs DA. Risk of Cataract Development among Children with Juvenile Idiopathic Arthritis-Related Uveitis Treated with Topical Corticosteroids. Ophthalmology. 2020; 127: S21–S26. https://doi.org/10.1016/j.ophtha.2020.01.036

[8] Zhao M, Zhang C, Chen XM, Teng Y, Shi TW, Liu F. Comparison of intravitreal injection of conbercept and triamcinolone acetonide for macular edema secondary to branch retinal vein occlusion. International Journal of Ophthalmology. 2020; 13: 1765–1772. https://doi.org/10.18240/ijo.2020.11.13

[9] Ginel J, Burguera N, Piñero D, Sáez-Martín A, Haro De Rosario A, Fernández J. Economic evaluations in cataract surgery: a narrative review. Eye (London, England). 2024; 38: 1418–1424. https://doi.org/10.1038/s41433-024-02965-x

[10] Kato K, Miyake K, Hirano K, Kondo M. Management of Postoperative Inflammation and Dry Eye After Cataract Surgery. Cornea. 2019; 38: S25–S33. https://doi.org/10.1097/ICO.0000000000002125

[11] Gangaputra S, Newcomb C, Ying GS, Groth S, Fitzgerald TD, Artornsombudh P, et al. Incidence and Remission of Post-Surgical Cystoid Macular Edema Following Cataract Surgery in Eyes With Intraocular Inflammation. American Journal of Ophthalmology. 2024; 267: 182–191. https://doi.org/10.1016/j.ajo.2024.06.006

[12] James ER. The etiology of steroid cataract. Journal of Ocular Pharmacology and Therapeutics: the Official Journal of the Association for Ocular Pharmacology and Therapeutics. 2007; 23: 403–420. https://doi.org/10.1089/jop.2006.0067

[13] Reimer R, Helmbold H, Szalay B, Hagel C, Hohenberg H, Deppert W, et al. Nestin modulates glucocorticoid receptor function by cytoplasmic anchoring. PloS One. 2009; 4: e6084. https://doi.org/10.1371/journal.pone.0006084

[14] Xie GL, Yan H, Lu ZF. Inhibition of glucocorticoid-induced changes of Na(+), K(+)-ATPase in rat lens by a glucocorticoid receptor antagonist RU486. Experimental Eye Research. 2010; 91: 544–549. https://doi.org/10.1016/j.exer.2010.07.005

[15] Celojevic D, Carlsson T, Johansson B, Nannmark U, Petersen A. Cell adhesion molecule expression in human lens epithelial cells after corticosteroid exposure. The Open Ophthalmology Journal. 2012; 6: 42–48. https://doi.org/10.2174/1874364101206010042

[16] Gupta V, Awasthi N, Wagner BJ. Specific activation of the glucocorticoid receptor and modulation of signal transduction pathways in human lens epithelial cells. Investigative Ophthalmology & Visual Science. 2007; 48: 1724–1734. https://doi.org/10.1167/iovs.06-0889

[17] Cui R, Cao G, Bai H, Zhang Z. LPAR1 regulates the development of intratumoral heterogeneity in ovarian serous cystadenocarcinoma by activating the PI3K/AKT signaling pathway. Cancer Cell International. 2019; 19: 201. https://doi.org/10.1186/s12935-019-0920-0

[18] Ping YQ, Mao C, Xiao P, Zhao RJ, Jiang Y, Yang Z, et al. Structures of the glucocorticoid-bound adhesion receptor GPR97-G_o complex. Nature. 2021; 589: 620–626. https://doi.org/10.1038/s41586-020-03083-w

[19] Andley UP, Rhim JS, Chylack LT, Jr, Fleming TP. Propagation and immortalization of human lens epithelial cells in culture. Investigative Ophthalmology & Visual Science. 1994; 35: 3094–3102.

[20] Chen S, Zhou Y, Chen Y, Gu J. fastp: an ultra-fast all-in-one FASTQ preprocessor. Bioinformatics (Oxford, England). 2018; 34: i884–i890. https://doi.org/10.1093/bioinformatics/bty560

[21] Kim D, Langmead B, Salzberg SL. HISAT: a fast spliced aligner with low memory requirements. Nature Methods. 2015; 12: 357–360. https://doi.org/10.1038/nmeth.3317

[22] Pertea M, Pertea GM, Antonescu CM, Chang TC, Mendell JT, Salzberg SL. StringTie enables improved reconstruction of a transcriptome from RNA-seq reads. Nature Biotechnology. 2015; 33: 290–295. https://doi.org/10.1038/nbt.3122

[23] Li B, Dewey CN. RSEM: accurate transcript quantification from RNA-Seq data with or without a reference genome. BMC Bioinformatics. 2011; 12: 323. https://doi.org/10.1186/1471-2105-12-323

[24] Love MI, Huber W, Anders S. Moderated estimation of fold change and dispersion for RNA-seq data with DESeq2. Genome Biology. 2014; 15: 550. https://doi.org/10.1186/s13059-014-0550-8

[25] Wang L, Feng Z, Wang X, Wang X, Zhang X. DEGseq: an R package for identifying differentially expressed genes from RNA-seq data. Bioinformatics (Oxford, England). 2010; 26: 136–138. https://doi.org/10.1093/bioinformatics/btp612

[26] Xie C, Mao X, Huang J, Ding Y, Wu J, Dong S, et al. KOBAS 2.0: a web server for annotation and identification of enriched pathways and diseases. Nucleic Acids Research. 2011; 39: W316–W322. https://doi.org/10.1093/nar/gkr483

[27] Ernst P, Baltzan M, Deschênes J, Suissa S. Low-dose inhaled and nasal corticosteroid use and the risk of cataracts. The European Respiratory Journal. 2006; 27: 1168–1174. https://doi.org/10.1183/09031936.06.00043005

[28] Daniel BS, Orchard D. Ocular side-effects of topical corticosteroids: what a dermatologist needs to know. The Australasian Journal of Dermatology. 2015; 56: 164–169. https://doi.org/10.1111/ajd.12292

[29] Petersen A, Carlsson T, Karlsson JO, Jonhede S, Zetterberg M. Effects of dexamethasone on human lens epithelial cells in culture. Molecular Vision. 2008; 14: 1344–1352.

[30] Petersen A, Zetterberg M. The Immunoproteasome in Human Lens Epithelial Cells During Oxidative Stress. Investigative Ophthalmology & Visual Science. 2016; 57: 5038–5045. https://doi.org/10.1167/iovs.16-19536

[31] Huang J, Yu W, He Q, He X, Yang M, Chen W, et al. Autophagy facilitates age-related cell apoptosis-a new insight from senile cataract. Cell Death & Disease. 2022; 13: 37. https://doi.org/10.1038/s41419-021-04489-8

[32] Eshagian J. Human posterior subcapsular cataracts. Transactions of the Ophthalmological Societies of the United Kingdom. 1982; 102 Pt 3: 364–368.

[33] Southren AL, Altman K, Vittek J, Boniuk V, Gordon GG. Steroid metabolism in ocular tissues of the rabbit. Investigative Ophthalmology. 1976; 15: 222–228.

[34] Eshaghian J, Streeten BW. Human posterior subcapsular

cataract. An ultrastructural study of the posteriorly migrating cells. Archives of Ophthalmology (Chicago, Ill.: 1960). 1980; 98: 134–143. https://doi.org/10.1001/archopht.1980.01020030136016

[35] Greiner JV, Chylack LT, Jr. Posterior subcapsular cataracts: histopathologic study of steroid-associated cataracts. Archives of Ophthalmology (Chicago, Ill.: 1960). 1979; 97: 135–144. https://doi.org/10.1001/archopht.1979.01020010069017

[36] Banerjee R, Hurtado Martínez JA, Flores Pérez PA, Porras N, Hydren J, Ahlstrom JM, et al. Association between dexamethasone exposure and visually significant cataracts in multiple myeloma. American Journal of Hematology. 2024; 99: E12–E14. https://doi.org/10.1002/ajh.27133

[37] Plüss CJ, Kustermann S. A Human Three-Dimensional In Vitro Model of Lens Epithelial Cells as a Model to Study Mechanisms of Drug-Induced Posterior Subcapsular Cataracts. Journal of Ocular Pharmacology and Therapeutics: the Official Journal of the Association for Ocular Pharmacology and Therapeutics. 2020; 36: 56–64. https://doi.org/10.1089/jop.2019.0010

[38] Manohar SM, Shah P, Nair A. Flow cytometry: principles, applications and recent advances. Bioanalysis. 2021; 13: 181–198. https://doi.org/10.4155/bio-2020-0267

[39] Donaldson PJ, Grey AC, Maceo Heilman B, Lim JC, Vaghefi E. The physiological optics of the lens. Progress in Retinal and Eye Research. 2017; 56: e1–e24. https://doi.org/10.1016/j.preteyeres.2016.09.002

[40] Liu Z, Huang S, Zheng Y, Zhou T, Hu L, Xiong L, et al. The lens epithelium as a major determinant in the development, maintenance, and regeneration of the crystalline lens. Progress in Retinal and Eye Research. 2023; 92: 101112. https://doi.org/10.1016/j.preteyeres.2022.101112

[41] Widomska J, Subczynski WK. Why Is Very High Cholesterol Content Beneficial for the Eye Lens but Negative for Other Organs? Nutrients. 2019; 11: 1083. https://doi.org/10.3390/nu11051083

[42] Rujoi M, Jin J, Borchman D, Tang D, Yappert MC. Isolation and lipid characterization of cholesterol-enriched fractions in cortical and nuclear human lens fibers. Investigative Ophthalmology & Visual Science. 2003; 44: 1634–1642. https://doi.org/10.1167/iovs.02-0786

[43] Chen X, Li P, Zhang G, Kang L, Qin B, Mao X, et al. Comprehensive Profiling of Proteome and Ubiquitome Changes in Human Lens Epithelial Cell Line after Ultraviolet-B Irradiation. ACS Omega. 2020; 5: 32171–32182. https://doi.org/10.1021/acsomega.0c03088

[44] Gong Y, Wei Q, Luo L, Qiu W, Jiang Y. A lipidomic study on the lens epithelial cells of patients with age related cataracts. PeerJ. 2024; 12: e17998. https://doi.org/10.7717/peerj.17998

[45] Zhou D, Zhang Y, Wang L, Sun Y, Liu P. Identification of genes and transcription factors associated with glucocorticoid response in lens epithelial cells. Molecular Medicine Reports. 2015; 11: 4073–4078. https://doi.org/10.3892/mmr.2015.3308

[46] James ER, Fresco VM, Robertson LL. Glucocorticoid-induced changes in the global gene expression of lens epithelial cells. Journal of Ocular Pharmacology and Therapeutics: the Official Journal of the Association for Ocular Pharmacology and Therapeutics. 2005; 21: 11–27. https://doi.org/10.1089/jop.2005.21.11

[47] Gupta V, Galante A, Soteropoulos P, Guo S, Wagner BJ. Global gene profiling reveals novel glucocorticoid induced changes in gene expression of human lens epithelial cells. Molecular Vision. 2005; 11: 1018–1040.

[48] Yang X, Kui L, Tang M, Li D, Wei K, Chen W, et al. High-Throughput Transcriptome Profiling in Drug and Biomarker Discovery. Frontiers in Genetics. 2020; 11: 19. https://doi.org/10.3389/fgene.2020.00019

[49] Guo Y, Sun Y, Zhang H. Advances in microbial transcriptomics techniques. Sheng Wu Gong Cheng Xue Bao. 2022; 38: 3606–3615. https://doi.org/10.13345/j.cjb.220527 (In Chinese)

[50] Kukurba KR, Montgomery SB. RNA Sequencing and Analysis. Cold Spring Harbor Protocols. 2015; 2015: 951–969. https://doi.org/10.1101/pdb.top084970

[51] Zhang Z, Lin X, Wei L, Wu Y, Xu L, Wu L, et al. A framework for Frizzled-G protein coupling and implications to the PCP signaling pathways. Cell Discovery. 2024; 10: 3. https://doi.org/10.1038/s41421-023-00627-y

[52] Dong Y, Zheng Y, Xiao J, Zhu C, Zhao M. MicroRNA let-7b induces lens epithelial cell apoptosis by targeting leucine-rich repeat containing G protein-coupled receptor 4 (Lgr4) in age-related cataract. Experimental Eye Research. 2016; 147: 98–104. https://doi.org/10.1016/j.exer.2016.04.018

[53] Zhu J, Hou Q, Dong XD, Wang Z, Chen X, Zheng D, et al. Targeted deletion of the murine Lgr4 gene decreases lens epithelial cell resistance to oxidative stress and induces age-related cataract formation. PloS One. 2015; 10: e0119599. https://doi.org/10.1371/journal.pone.0119599

[54] Xiao D, Su X, Gao H, Li X, Qu Y. The Roles of Lpar1 in Central Nervous System Disorders and Diseases. Frontiers in Neuroscience. 2021; 15: 710473. https://doi.org/10.3389/fnins.2021.710473

[55] Lu CL, Ren J, Mo JW, Fan J, Guo F, Chen LY, et al. Glucocorticoid Receptor-Dependent Astrocytes Mediate Stress Vulnerability. Biological Psychiatry. 2022; 92: 204–215. https://doi.org/10.1016/j.biopsych.2021.11.022

[56] Gomez-Larrauri A, Gangoiti P, Presa N, Dominguez-Herrera A, Donati C, Bruni P, et al. Phosphatidic Acid Stimulates Myoblast Proliferation through Interaction with LPA1 and LPA2 Receptors. International Journal of Molecular Sciences. 2021; 22: 1452. https://doi.org/10.3390/ijms22031452

[57] Zhang J, Li Y, Wang C, Wang Y, Zhang Y, Huang L, et al. Lysophosphatidic Acid Induces Apoptosis of PC12 Cells Through LPA1 Receptor/LPA2 Receptor/MAPK Signaling Pathway. Frontiers in Molecular Neuroscience. 2020; 13: 16. https://doi.org/10.3389/fnmol.2020.00016

[58] Sevilla LM, Jiménez-Panizo A, Alegre-Martí A, Estébanez-Perpiñá E, Caelles C, Pérez P. Glucocorticoid Resistance: Interference between the Glucocorticoid Receptor and the MAPK Signalling Pathways. International Journal of Molecular Sciences. 2021; 22: 10049. https://doi.org/10.3390/ijms221810049

[59] Yu H, Guo Y, Zhao Y, Zhou F, Zhao K, Li M, et al. Both insufficient and excessive glucocorticoid receptor-mediated signaling impair neuronal migration. The Journal of Endocrinology. 2019; 242: 103–114. https://doi.org/10.1530/JOE-19-0207

[60] Juin A, Spence HJ, Martin KJ, McGhee E, Neilson M, Cutiongco MFA, et al. N-WASP Control of LPAR1 Trafficking Establishes Response to Self-Generated LPA Gradients to Promote Pancreatic Cancer Cell Metastasis. Developmental Cell. 2019; 51: 431–445.e7. https://doi.org/10.1016/j.devcel.2019.09.018

[61] Zhang HP, Jiang RY, Zhu JY, Sun KN, Huang Y, Zhou HH, et al. PI3K/AKT/mTOR signaling pathway: an important driver and therapeutic target in triple-negative breast cancer. Breast Cancer (Tokyo, Japan). 2024; 31: 539–551. https://doi.org/10.1007/s12282-024-01567-5

[62] Glaviano A, Foo ASC, Lam HY, Yap KCH, Jacot W, Jones RH, et al. PI3K/AKT/mTOR signaling transduction pathway and targeted therapies in cancer. Molecular Cancer. 2023; 22: 138. https://doi.org/10.1186/s12943-023-01827-6

[63] Nazmy MH, Abu-Baih DH, Elrehany MA, Mustafa M, Aly OM, El-Sheikh AAK, et al. Assessing the Antiproliferative Potential of a Novel Combretastatin A4 Derivative via Modulating Apoptosis, MAPK/ERK and PI3K/AKT Pathways in Human Breast Cancer Cells. Frontiers in Bioscience (Landmark Edition). 2023;

28: 185. https://doi.org/10.31083/j.fbl2808185

[64] Hall MA, Verma SS, Wallace J, Lucas A, Berg RL, Connolly J, *et al*. Biology-Driven Gene-Gene Interaction Analysis of Age-Related Cataract in the eMERGE Network. Genetic Epidemiology. 2015; 39: 376–384. https://doi.org/10.1002/gepi.21902

[65] Du L, Hao M, Li C, Wu W, Wang W, Ma Z, *et al*. Quercetin inhibited epithelial mesenchymal transition in diabetic rats, high-glucose-cultured lens, and SRA01/04 cells through transforming growth factor-β2/phosphoinositide 3-kinase/Akt pathway. Molecular and Cellular Endocrinology. 2017; 452: 44–56. https://doi.org/10.1016/j.mce.2017.05.011

[66] Qin Y, Zhu Y, Luo F, Chen C, Chen X, Wu M. Killing two birds with one stone: dual blockade of integrin and FGF signaling through targeting syndecan-4 in postoperative capsular opacification. Cell Death & Disease. 2017; 8: e2920. https://doi.org/10.1038/cddis.2017.315

[67] Wang J, Wang R, Wang H, Yang X, Yang J, Xiong W, *et al*. Glucocorticoids Suppress Antimicrobial Autophagy and Nitric Oxide Production and Facilitate Mycobacterial Survival in Macrophages. Scientific Reports. 2017; 7: 982. https://doi.org/10.1038/s41598-017-01174-9

[68] Costello MJ, Brennan LA, Basu S, Chauss D, Mohamed A, Gilliland KO, *et al*. Autophagy and mitophagy participate in ocular lens organelle degradation. Experimental Eye Research. 2013; 116: 141–150. https://doi.org/10.1016/j.exer.2013.08.017

[69] Ma J, Ye W, Yang Y, Wu T, Wang Y, Li J, *et al*. The interaction between autophagy and the epithelial-mesenchymal transition mediated by NICD/ULK1 is involved in the formation of diabetic cataracts. Molecular Medicine (Cambridge, Mass.). 2022; 28: 116. https://doi.org/10.1186/s10020-022-00540-2

[70] Massa H, Georgoudis P, Panos GD. Dexamethasone intravitreal implant (OZURDEX®) for macular edema secondary to noninfectious uveitis: a review of the literature. Therapeutic Delivery. 2019; 10: 343–351. https://doi.org/10.4155/tde-2019-0024

[71] Corte TJ, Lancaster L, Swigris JJ, Maher TM, Goldin JG, Palmer SM, *et al*. Phase 2 trial design of BMS-986278, a lysophosphatidic acid receptor 1 (LPA$_1$) antagonist, in patients with idiopathic pulmonary fibrosis (IPF) or progressive fibrotic interstitial lung disease (PF-ILD). BMJ Open Respiratory Research. 2021; 8: e001026. https://doi.org/10.1136/bmjresp-2021-001026

[72] Konopa A, Meier MA, Franz MJ, Bernardinelli E, Voegele AL, Atreya R, *et al*. LPA receptor 1 (LPAR1) is a novel interaction partner of Filamin A that promotes Filamin A phosphorylation, MRTF-A transcriptional activity and oncogene-induced senescence. Oncogenesis. 2022; 11: 69. https://doi.org/10.1038/s41389-022-00445-z

[73] Holland EJ, Fingeret M, Mah FS. Use of Topical Steroids in Conjunctivitis: A Review of the Evidence. Cornea. 2019; 38: 1062–1067. https://doi.org/10.1097/ICO.0000000000001982

[74] Liu LC, Chen YH, Lu DW. Overview of Recent Advances in Nano-Based Ocular Drug Delivery. International Journal of Molecular Sciences. 2023; 24: 15352. https://doi.org/10.3390/ijms242015352

[75] Onugwu AL, Nwagwu CS, Onugwu OS, Echezona AC, Agbo CP, Ihim SA, *et al*. Nanotechnology based drug delivery systems for the treatment of anterior segment eye diseases. Journal of Controlled Release: Official Journal of the Controlled Release Society. 2023; 354: 465–488. https://doi.org/10.1016/j.jconrel.2023.01.018

[76] Wei J, Mu J, Tang Y, Qin D, Duan J, Wu A. Next-generation nanomaterials: advancing ocular anti-inflammatory drug therapy. Journal of Nanobiotechnology. 2023; 21: 282. https://doi.org/10.1186/s12951-023-01974-4

[77] Tian Y, Zhang T, Li J, Tao Y. Advances in development of exosomes for ophthalmic therapeutics. Advanced Drug Delivery Reviews. 2023; 199: 114899. https://doi.org/10.1016/j.addr.2023.114899

[78] Xie M, Wu Y, Zhang Y, Lu R, Zhai Z, Huang Y, *et al*. Membrane Fusion-Mediated Loading of Therapeutic siRNA into Exosome for Tissue-Specific Application. Advanced Materials (Deerfield Beach, Fla.). 2024; 36: e2403935. https://doi.org/10.1002/adma.202403935

[79] Jiang W, Xiao D, Wu C, Yang J, Peng X, Chen L, *et al*. Circular RNA-based therapy provides sustained and robust neuroprotection for retinal ganglion cells. Molecular Therapy. Nucleic Acids. 2024; 35: 102258. https://doi.org/10.1016/j.omtn.2024.102258

[80] Yu F, Gong D, Yan D, Wang H, Witman N, Lu Y, *et al*. Enhanced adipose-derived stem cells with IGF-1-modified mRNA promote wound healing following corneal injury. Molecular Therapy: the Journal of the American Society of Gene Therapy. 2023; 31: 2454–2471. https://doi.org/10.1016/j.ymthe.2023.05.002

[81] Li Q, Liu S, Yang G, Li M, Qiao P, Xue Q. Naringenin inhibits autophagy and epithelial-mesenchymal transition of human lens epithelial cells by regulating the Smad2/3 pathway. Drug Development Research. 2022; 83: 389–396. https://doi.org/10.1002/ddr.21868

[82] Choi GE, Han HJ. Glucocorticoid impairs mitochondrial quality control in neurons. Neurobiology of Disease. 2021; 152: 105301. https://doi.org/10.1016/j.nbd.2021.105301